Integrated DES Leaching and Mn-Selective Solvent Extraction for $MnCO_3$ Precursor Production from Used Lithium-Ion Battery Cathodes

Jafar Goudarzi

A Thesis in The

Department of

Building, Civil and Environmental Engineering

Presented in Partial Fulfillment of the Requirements

for the Degree of Master of Applied Science (Environmental Engineering) at

Concordia University

Montreal, Quebec, Canada

March 2026

CONCORDIA UNIVERSITY

School of Graduate Studies

This is to certify that the thesis

prepared By: Jafar Goudarzi

Entitled: Integrated DES Leaching and Mn-Selective Solvent Extraction for $MnCO_3$ Precursor Production from Used Lithium-Ion Battery Cathodes

and submitted in partial fulfillment of the requirements for the degree of

Master of Applied Science (Environmental Engineering)

complies with the regulations of the University and meets the accepted standards with respect to originality and quality.

Signed by the final Examining Committee:

Chair	Dr. Chunjiang An
Examiner	Dr. Chunjiang An
Examiner	Dr. Jaehoon Hwang
Supervisor	Dr. Zhi Chen

Approved by

Chair of Department or Graduate Program Director

2026

Dean of Faculty

Abstract

The increased usage of EVs will result in rising quantities of end-of-life LIBs. This requires recycling processes capable of recovering valuable metals while minimizing associated environmental impacts. Established metallurgical processes for Li extraction utilize hydro- and pyrometallurgical approaches involving concentrated mineral acids and several separation steps. In addition, emerging deep eutectic solvents (DESs) show promise in tailoring coordination chemistry for effective metal leaching. However, much of the available DES-related literature tends to focus on leaching performances and rarely on downstream process stages aimed at obtaining the desired precursor product. Therefore, the present study aims to fill this knowledge gap by developing an approach towards Mn "leach-to-precursor" via DES leaching, Mn-specific solvent extraction (SX), and $MnCO_3$ precipitation.

Two related experimental systems were established. Firstly, a choline chloride-D-glucose DES modified by 10 wt.% water was investigated for efficient dissolution of Mn-containing spent cathodes to enhance mass transfer while retaining DES characteristics. Under optimal conditions, nearly 100% dissolution was obtained for lithium and manganese, compared to 71% dissolution of nickel. Secondly, selective Mn extraction from multicomponent Mn-Co-Ni-Li DES extractant solution was achieved using D2EHPA in kerosene. Under optimal conditions, Mn extraction reached 89.7%, with low cobalt and nickel co-extraction and large separation factors ($\beta Mn/Co = 143$; $\beta Mn/Ni = 208$). Two-step acid stripping resulted in 94.8% Mn recovery, whereas carbonate precipitation under neutral pH (7-8) yielded rhodochrosite $MnCO_3$ with 95.3% Mn precipitation recovery and overall recovery of 81.0%.

Acknowledgments

I would like to take this opportunity to acknowledge the many individuals whose support contributed to the completion of this thesis. I am grateful to Concordia University for providing an enriching academic setting, access to essential facilities, and a research environment that encouraged growth and learning throughout my master's program.

I am profoundly thankful to my supervisor, Prof. Zhi Chen, for his guidance, insightful feedback, and steady encouragement during every stage of this work. His expertise and thoughtful direction helped me strengthen my research approach, refine my writing, and maintain a clear focus on the objectives of the project. I truly appreciate his time, patience, and the high standards he continuously inspired.

Above all, I would like to offer my special thanks to my wife, whose understanding, patience, and unwavering support carried me through the most demanding moments of this journey. Her encouragement, kindness, and belief in my abilities gave me the strength to stay focused and persevere. This achievement would not have been possible without her constant presence and support.

CONTENTS

List of Figures

List of Tables

CHAPTER 1 INTRODUCTION

1.1 Motivation

Modern electrified systems, from grid storage and electric vehicles (EVs) to portable gadgets and data center backup, are powered by lithium-ion batteries (LIBs). The rapid growth of EVs and stationary energy storage has accelerated the generation of end-of-life (EoL) LIBs, increasing pressure on recycling systems to recover critical metals while reducing environmental burdens and safety risks associated with spent cells (Or et al. 2020; Rehman et al. 2025). At EoL, LIBs represent both an environmental liability and a strategic urban resource: they contain valuable and supply-critical materials including Li, Ni, Co, Mn, and conductive/current-collector metals that can be recovered to mitigate primary mining demand and supply-chain risks (Asadi Dalini et al. 2020; Or et al. 2020).

Commercial LIBs typically consist of a cathode coating on Al foil, a graphite anode on Cu foil, a porous polymer separator, and a $LiPF_6$-based organic electrolyte (Xu 2004). Industrial pretreatment of EoL cells often produces a cathode-rich “black mass” (BM)—a heterogeneous powder containing active materials, conductive carbon, binder residues, and variable levels of Al/Cu impurities (Milian et al. 2024). Because downstream separation performance depends strongly on feed chemistry and impurity carryover, credible recycling studies should address realistic multicomponent feeds and report results using auditable stream compositions (Gilligan, O’Malley, and Nikoloski 2025; Milian et al. 2024). Policy developments (e.g., recycled-content and recycling-efficiency expectations) further reinforce the need for selective, resource-efficient flowsheets capable of producing reintegration-ready precursor materials.

Industrial LIB recycling is currently dominated by pyrometallurgy and hydrometallurgy. Pyrometallurgy is robust to feed variability and simplifies handling of organics, but typically requires high energy input, provides limited intrinsic selectivity, and may partition lithium into slag, often necessitating subsequent hydrometallurgical refining (Cornelio et al. 2024; Makuza et al. 2021). Hydrometallurgy enables selective recovery at moderate temperatures through leaching followed by separation steps such as precipitation, solvent extraction (SX), ion exchange, electrowinning, and crystallization (Y. Wang et al. 2020). However, mineral-acid routes can be reagent-intensive and generate wastewater-treatment burdens and salt-laden neutralization residues (Asadi Dalini et al. 2020; Y. Wang et al. 2020). Organic acids have been explored as greener alternatives, yet high recoveries and industrially relevant kinetics may require intensified conditions or added reductants, increasing cost and complexity (Golmohammadzadeh et al. 2017; Rouquette et al. 2023). These considerations motivate alternative leaching media that can combine effective dissolution with improved selectivity potential and reduced secondary waste generation.

Deep eutectic solvents (DESs) have gained attention as alternative leaching media because they can dissolve transition metals under comparatively mild conditions and can be formulated from inexpensive components (Tran et al. 2019). Recent work highlights both opportunities and challenges: solvent design (HBA/HBD selection), water content, viscosity, and stability during cycling can strongly influence dissolution, metal speciation, and compatibility with downstream purification (Fan et al. 2023; Zhu et al. 2023). Broader hydrometallurgical perspectives further emphasize that DES-based recycling must demonstrate credible solvent/stream management and process-relevant unit operations rather than dissolution-only performance (Martín et al. 2023). Mechanistic studies also

indicate that metal–DES interactions can differ across chemistries, reinforcing the need for integrated demonstrations that connect leaching to separation and product outcomes (Behnajady et al. 2024; Wang et al. 2023).

Accordingly, there is a practical need to move beyond leaching-only demonstrations toward integrated, Mn flowsheets that couple DES dissolution with selective downstream separations and conversion to a defined precursor product suitable for reintegration into battery-material supply chains.

1.2 Study Objectives

Historically, recycling value propositions prioritized cobalt and lithium, while manganese was often treated as a lower-value component or diluted into mixed products (Chan et al. 2021). This landscape is changing as Mn-containing cathodes remain important for balancing cost, safety, and performance, and as Mn becomes increasingly relevant for resilient battery supply chains (Chan et al. 2021). Targeting manganese carbonate ($MnCO_3$) is attractive because it is a concentrated, handleable solid product and a useful precursor/intermediate for Mn-based cathode-material production routes. In many conventional routes, Mn is recovered as $MnSO_4$ (or remains within mixed streams), which can require additional conversion steps to reach $MnCO_3$ or other Mn products, increasing unit operations and chemical consumption (Locati et al. 2024). While simplified aqueous schemes such as ammonia-based approaches can enable $MnCO_3$ formation, their compatibility with DES-derived matrices and selectivity control under multicomponent conditions are not guaranteed (C. Wang et al. 2020).

A central bottleneck in Mn recycling is the selective separation of Mn^{2+} from Co^{2+} and Ni^{2+} in multicomponent leach liquors, where these transition metals can show comparable coordination tendencies under many conditions (Chan et al. 2021; Locati et al. 2024). Among industrially established extractants, organophosphorus acids such as di-(2-ethylhexyl) phosphoric acid (D2EHPA) can preferentially extract Mn at relatively low pH while suppressing Co and Ni extraction within an operating window; however, separation performance depends strongly on pH, degree of saponification, extractant concentration, organic-to-aqueous phase ratio (O/A), and phase conditioning (Keller et al. 2021; Nadimi and Karazmoudeh 2021; Vieceli et al. 2020; Yun, Wen, and Lee 2024).

In the DES recycling literature, a recurring gap is that many studies emphasize dissolution efficiency but do not implement integrated downstream separations that deliver a well-defined Mn precursor from realistic DES-derived feeds. Reviews highlight that translating DES leaching into robust flowsheets requires careful management of dilution strategies, phase behavior, and compatibility with purification steps while minimizing intermediate conversions and demonstrating auditable product streams (Rautela et al. 2023; Su et al. 2024). Therefore, there remains a practical need for a process that (i) is compatible with DES-derived leachates, (ii) selectively isolates Mn from Co/Ni/Li under realistic multicomponent conditions, and (iii) directly delivers $MnCO_3$ with minimal intermediate processing.

Accordingly, this thesis frames Mn recovery as an integrated leach → separation → precursor problem. The work employs a sugar-based DES (Choline Chloride, D-glucose) with controlled water addition to reduce viscosity and improve mass transfer, combined with Mn-selective D2EHPA extraction, acid stripping, and carbonate

precipitation to $MnCO_3$. Building on prior work demonstrating effective dissolution in a water-modified ChCl:D-glucose DES (Goudarzi et al. 2025), the thesis focuses on (1) quantifying the effects of leaching temperature/time on metal dissolution, (2) establishing Mn-selective extraction and Mn/Co–Mn/Ni separation under controlled conditions, and (3) verifying $MnCO_3$ formation and reporting product/stream quality using structural and ICP-based analytics.

1.3 Thesis Organization

This thesis follows a two-work thesis format. To minimize repetition across the experimental chapters, common materials, methods, and experimental setup are consolidated in a dedicated methodology chapter. The experimental chapters then focus primarily on results and discussion and include only brief, chapter-specific procedural notes where needed.

Chapter 1 introduces the motivation, research gap, and scope for Mn recovery to $MnCO_3$. Chapter 2 reviews the LIB recycling context and prior work on DES leaching and post-leach separations relevant to Mn selectivity and precursor production. Chapter 3 compiles the common methodology and experimental setup, including feedstock preparation, DES formulation, leaching procedures, analytical methods, and general solvent extraction/precipitation protocols. Chapters 4 and 5 present the experimental results and discussion for the two linked parts of the work, with minimal chapter-specific methodological details included only when necessary for clarity. Chapter 6 provides an integrated discussion and benchmarking against representative literature. Chapter 7 summarizes the thesis conclusions, key contributions, and directions for future work.

CHAPTER 2 LITERATURE REVIEW

2.1 Overview

High specific energy, power density, and cycle life have established lithium-ion batteries (LIBs) as the dominant technology for portable electronics, electric vehicles (EVs), and stationary storage. Rapid expansion of EV deployment and grid storage is accelerating end-of-life (EoL) battery flows and driving demand for recycling strategies that recover valuable metals (Li, Co, Ni, Mn) while reducing environmental burdens and safety risks. Recent reviews emphasize that scalable recycling requires robust unit operations, auditable product quality, and flowsheets compatible with a circular-economy framework and evolving policy expectations (Baum et al. 2022; Harper et al. 2019; Latini et al. 2022; Neumann et al. 2022; Srivastava et al. 2023; Velázquez-Martínez et al. 2019).

Conventional industrial recycling routes are dominated by pyrometallurgy and hydrometallurgy. Pyrometallurgy is robust to feed variability but is energy-intensive and often requires downstream hydrometallurgical refining to achieve high-purity products (Cornelio et al. 2024; Harper et al. 2019; Makuza et al. 2021; Neumann et al. 2022). Hydrometallurgy provides separation flexibility through leaching followed by solvent extraction (SX), precipitation, crystallization, and electrochemical steps, but mineral acid systems can be reagent-intensive and impose significant wastewater/neutralization burdens (Gaines 2018; Lei, Sun, and Yang 2022; Shin et al. 2005; Y. Wang et al. 2020). Organic-acid leaching can reduce corrosivity but may require intensification to achieve competitive kinetics and high yields (Golmohammadzadeh et al. 2017; Rouquette et al. 2023).

In parallel, deep eutectic solvents (DESs) have emerged as promising leaching media due to low volatility, tunable coordination chemistry, and the potential to reduce secondary

pollution while enabling solvometallurgical flowsheets (Fan et al. 2023; Martín et al. 2023; Tran et al. 2019; Zhu et al. 2023). Multiple reviews highlight that the key challenge is moving beyond "leaching-only" demonstrations toward integrated routes that manage viscosity/hydration, maintain solvent performance, and connect dissolution to credible downstream separations and product streams (Martín et al. 2023; Rautela et al. 2023; Su et al. 2024; Zhu et al. 2023).

This thesis targets Mn recovery culminating in $MnCO_3$ as a defined precursor product. Achieving selective Mn^{2+} separation from Co^{2+}/Ni^{2+} in multicomponent liquors remains challenging, but industrially established extractants (notably D2EHPA) can preferentially extract Mn in a suitable pH window (Keller et al. 2021; Nadimi and Karazmoudeh 2021; Vieceli et al. 2020; Yun et al. 2024). $MnCO_3$ production is attractive because it delivers a concentrated, handleable solid that is relevant to cathode precursor value chains and can be produced via carbonate precipitation once a sufficiently pure Mn stream is obtained (C. Wang et al. 2020). Accordingly, this chapter synthesizes (i) LIB feedstock and black-mass characteristics, (ii) pretreatment strategies and conventional recovery pathways, (iii) DES fundamentals and design levers, and (iv) DES-enabled leaching and post-leach separations, with emphasis on gaps relevant to integrated $MnCO_3$ production.

2.2 Feedstock, Black Mass, Pretreatment, and Conventional Recycling Routes

LIBs typically comprise a cathode coating (active oxide + conductive carbon + binder) on an Al current collector, a graphite anode on a Cu collector, a porous polyolefin separator, and a non-aqueous electrolyte (often $LiPF_6$ in carbonate solvent blends) (Harper

et al. 2019; Xu 2004). Cathode chemistry dictates the distribution/speciation of valuable metals and impurities in recycling streams; common families include layered oxides (e.g., LCO, NMC, NCA), spinel LMO, and olivine LFP, which drive different Ni/Co/Mn/Li inventories and downstream separation requirements (Baum et al. 2022; Harper et al. 2019; Neumann et al. 2022).

At EoL, industrial pretreatment typically produces a cathode-rich powder fraction commonly termed black mass (BM). BM is heterogeneous, containing cathode and anode powders, conductive carbon, binder residues, and electrolyte-derived salts, with variable Al/Cu fines from foil fragmentation. This variability directly influences leach reagent demand, impurity control, and separation operability (Latini et al. 2022; Neumann et al. 2022). Recent reviews emphasize that realistic BM feeds can introduce additional complexity (graphite-rich solids affecting slurry handling and filtration; increased impurity carryover), making integrated, stream-auditable demonstrations essential (Gilligan et al. 2025; Latini et al. 2022; Milian et al. 2024; Neumann et al. 2022).

High-level overview of the three dominant recycling routes

Across the literature, LIB recycling routes are commonly grouped into pyrometallurgy, hydrometallurgy, and direct recycling (or "cathode-to-cathode" regeneration). Table 2-1 provides an indicative comparison of their typical unit operations, strengths/limitations, product forms, and maturity as synthesized from representative reviews (Baum et al. 2022; Cornelio et al. 2024; Makuza et al. 2021; Srivastava et al. 2023).

Table 2-1. Overview of LIB recycling routes and typical outputs (indicative; review-based)

Route	Typical operations	Main reagents/conditions	Strengths	Limitations	Typical products	Indicative Refs
Pyrometallurgy	Discharge → shredding/drying → smelting/roasting (≈1200–1500 °C) → alloy/matte + slag handling → (often) hydro-refining	Fluxes (e.g., CaO/SiO_2); reductants (C/coke); high T; off-gas treatment	Robust to heterogeneous feeds; handles organics; simple solids handling	High energy demand; off-gas/slag management; limited intrinsic selectivity; Li often partitions to slag → needs downstream refining	Co/Ni/Cu-rich alloy/matte; Li-enriched slag; mixed residues	(Cornelio et al. 2024; Harper et al. 2019; Makuza et al. 2021; Neumann et al. 2022)
Hydrometallurgy	BM prep → acid/alkali leach (often + reductant) → SX / precipitation /	Mineral acids (H_2SO_4/HCl) and/or organic acids;	High recovery & product purity potential;	Reagent-intensive; wastewater/neutralization burdens; multi-step complexity	Battery-grade Li_2CO_3/LiOH; Ni/Co salts; Mn salts;	(Asadi Dalini et al. 2020; Gaines

	ion exchange → crystallization / electrowinning	oxidant/reductant as needed; moderate T	modular/selective separations; lower T than pyro		precursor solutions	2018; Shin et al. 2005; Y. Wang et al. 2020)
Direct recycling	Pretreat → delamination → separation by chemistry/grade → relithiation/regeneration (thermal/hydrothermal) → re-qualification	Controlled atmospheres; relithiation agents (Li salts); moderate-high T depending on route	Preserves cathode structure; potential energy/cost savings; fewer chemical conversions	Requires sorting by chemistry; impurity/binder control; quality assurance and scale-up challenges	Regenerated cathode powders (NMC/LCO etc.)	(Latini et al. 2022; Neumann et al. 2022; Srivastava et al. 2023)

Pretreatment as the practical bridge from packs/cells to processable BM

Pretreatment transforms EoL LIBs into physically and chemically processable feedstocks. Reviews consistently identify core objectives as safe deactivation, liberation of electrode coatings, removal of coarse Al/Cu fractions, and production of a particle-size distribution that supports efficient leaching and solid–liquid separation (Kim et al. 2021; Latini et al. 2022; Neumann et al. 2022; Zhang et al. 2021). Safety is first-order because EoL cells may retain residual charge and flammable electrolyte; aqueous discharge has been explored, but can introduce secondary risks (gas evolution, corrosion, metal dissolution/redeposition) unless carefully controlled (Ojanen et al. 2018; Shaw-Stewart et al. 2019).

A key pretreatment step is electrode liberation/delamination (separating coatings from Al/Cu foils) and binder management. Greener delamination approaches using alternative solvents and tailored conditions have been demonstrated, and physical intensification (e.g., ultrasonication) can accelerate coating removal with limited chemical consumption (Buken et al. 2021; Lei et al. 2021). Thermal/chemical routes for PVDF removal and delamination are also reported but require careful control of fluorinated emissions and waste streams (Ji et al. 2022). Particle-size control (crushing, milling, sieving) is widely recognized as a major lever affecting leaching kinetics, filtration, and SX operability; overly fine material can hinder solid–liquid separation, while insufficient comminution leaves composite laminates that leach poorly (Latini et al. 2022; Neumann et al. 2022; Takahashi et al. 2020).

Overall, the literature supports three implications for Mn flowsheets: (i) BM variability must be explicitly characterized; (ii) pretreatment choices affect impurity carryover (Al/Cu/F-containing species) that can compromise selectivity and product purity; and (iii) downstream separations must be designed for multicomponent matrices rather than idealized single-oxide powders (Latini et al. 2022; Rensmo et al. 2023).

2.3 Deep Eutectic Solvents for LIB Recycling

DESs are liquids formed by complexation of a hydrogen-bond acceptor (HBA) and a hydrogen-bond donor (HBD) at defined ratios, yielding melting-point depression and strong solvation/coordination behavior relative to the pure components (Abbott et al. 2004, 2006; Dai et al. 2013; Smith et al. 2014; Zhang et al. 2012). For metal processing, DESs offer low vapor pressure and broad tunability, and are widely reviewed as alternatives to conventional aqueous leachants and ionic liquids (Dai et al. 2013; Smith et al. 2014; Zhang et al. 2012). “Natural” deep eutectic solvents (NADES) based on bio-derived components (e.g., acids, amino acids, sugars) can increase renewability and may offer favorable safety profiles depending on formulation (Gygli, Xu, and Pleiss 2020).

For LIB recycling, DES performance is governed by a set of coupled design levers acidity/coordination strength, viscosity and mass-transfer constraints, water content, and speciation/redox environment (Fan et al. 2023; Martín et al. 2023; Tran et al. 2019; Zhu et al. 2023). Viscosity is a central engineering constraint: it decreases strongly with temperature and with controlled water addition, but the response is non-linear and composition-dependent (Hammond et al. 2023; Rozas et al. 2021). Importantly, even trace water can shift metal-ion speciation and clustering in DES media, potentially changing extraction selectivity and phase behavior reinforcing the need to define and control a

practical “water window” (Dong et al. 2023). These considerations are particularly relevant to glucose-based DESs (e.g., ChCl:D-glucose), where controlled hydration reduces viscosity and improves mass transfer while influencing coordination/redox behavior (Behnajady et al. 2024; Goudarzi et al. 2025). In this thesis, the water content was fixed at 10 wt.% (literature-informed) and evaluated through comparison of binary vs. water-modified formulations; systematic mapping of the broader “water window” and viscosity measurements were beyond scope and are recommended as future work.

Against this background, DESs have been widely investigated for leaching Li and transition metals from spent cathode materials, particularly NMC-type feeds. The foundational perspective by Tran et al. highlighted solvometallurgical opportunities and emphasized the need for integrated, unit-operation-realistic flowsheets (Tran et al. 2019). Subsequent reviews consolidate that high dissolution efficiencies can be achieved under moderate-to-elevated temperatures depending on DES acidity, viscosity, hydration, solid loading, and mixing (Fan et al. 2023; Martín et al. 2023; Zhu et al. 2023). However, reviews consistently caution that “leaching-only” results are insufficient: downstream phase management, solvent cycling, and conversion to defined product streams are necessary to demonstrate process credibility (Martín et al. 2023; Rautela et al. 2023; Su et al. 2024; Zhu et al. 2023). Accordingly, Table 2-2 compiles representative experimentally specified DES leaching studies (selected, leaching-focused) and highlights how formulation and operating windows influence performance.

Table 2-2. Representative DES formulations and operating windows for leaching of spent LIB cathodes (selected examples).

Feed/cathode	DES (HBA: HBD; indicative)	Water in DES	T (°C)	t	Solid loading (indicative)	Key outcome (indicative)	Notes	Ref.
LiMn-based cathode material (Mn-rich)	ChCl:D-glucose (2:1) NADES	10 wt.% (added; viscosity control)	60–110	2–24 h	~10 g/L (50 mg in 5 mL DES)	Reported high Li and Mn dissolution under optimized conditions (e.g., Li ~98.9%, Mn ~98.4%)	Sugar-based DES; hydration strongly impacts viscosity/mass transfer	(Goudarzi et al. 2025)

LCO and NMC cathodes	Ethylene glycol:oxalic acid dihydrate (e.g., 5EG:1OAD)	Inherent (from oxalic acid dihydrate; ~10 wt.% noted in source)	~90	~12 h	~16 g/L (reported)	Selective Li leaching to solution (~94% Li) with limited Co/Ni/Mn dissolution (<~1.2%); Co/Ni/Mn captured as oxalate solids	"Bifunctional" leach + in situ separation concept	(Tang et al. 2022)
Spent NCM cathode material	Ethylene glycol–malonic acid acidic DES (EG:MA ≈3–4:1, reported)	Not reported	~90	~6 h	~30 g/L	High leaching efficiencies reported (Li ~92.8%, Co ~93.7%, Ni ~89.5%, Mn ~91.4%)	Low-viscosity acidic DES aimed at improving mass transfer	(Zhang et al. 2022)

NCM523-type cathode powder	Betaine HCl:ethylene glycol (1:5) (acidic DES)	Not specified	100–160	1–20 min	0.5 g in 20 g DES (~25 g per kg DES)	Near-complete dissolution reported at elevated temperature (e.g., ~140 °C; Li/Co/Ni/Mn ≈99%+)	High-T, short-time dissolution; emphasizes kinetics	(Luo et al. 2022)

2.4 Recovery Pathways and Separation Logic for Manganese in DES Media

A major bottleneck for DES-enabled recycling is post-leach separation and delivery of defined products. Reviews emphasize two recurring strategies: (i) transfer of metals from DES into an aqueous phase (via dilution/stripping/phase manipulation) followed by conventional hydrometallurgical separations; and/or (ii) recovery from DES–water systems using SX/electrochemical/hybrid routes, which requires careful control of phase behavior and speciation (Martín et al. 2023; Rautela et al. 2023; Su et al. 2024; Zhu et al. 2023).

For Mn routes, selective Mn recovery is most demonstrated using acidic organophosphorus extractants. D2EHPA is industrially relevant due to favorable Mn distribution at relatively low pH and the potential for high Mn/Co and Mn/Ni separation within a controlled operating window (Keller et al. 2021; Nadimi and Karazmoudeh 2021; Vieceli et al. 2020; Yun et al. 2024). Once a sufficiently purified Mn stream is produced (often after stripping to an aqueous sulfate/chloride medium), $MnCO_3$ can be produced via carbonate precipitation as a concentrated, handleable precursor (C. Wang et al. 2020). Table 2-3 summarizes representative recovery/separation steps that are directly relevant to Mn-selective circuits (including cases where DES leaching is followed by aqueous separation logic).

Table 2-3. Representative post-leach separations for Mn recovery and $MnCO_3$ precursor production (SX/precipitation/electrochemical; selected examples).

System/stream	Recovery step	Key conditions (indicative)	Target/outcome	Key takeaway	Ref.
Synthetic or LIB-based leach liquor (Mn/Co-containing)	Mn-selective SX with D2EHPA + scrubbing + stripping	0.5 M D2EHPA, pH 3.25, O:A = 1.25:1; Mn extraction >70% in one stage with <5% Co co-extraction; Co mostly removed by two scrubbing stages; stripping can yield ~23 g/L Mn with ~0.3 g/L Co using 1 M H_2SO_4, O:A = 8:1, ~13 min	Preferential Mn transfer to organic; Mn-rich strip liquor after stripping	Quantifies sensitivity to pH and phase ratio and shows how scrubbing/stripping upgrades product quality	(Vieceli et al. 2020)

Co/Mn/Ni sulfate media (LIB leach-derived)	Staged / counter-current SX (Cyanex 272 → D2EHPA)	1st: 0.3 M Cyanex 272 (40% saponified) extracts Co + Mn in one stage, leaving Ni in raffinate ; Ni removed by two-stage scrubbing with $CoSO_4$ solution ; Co/Mn stripped with 0.05 M H_2SO_4 ; then three-stage counter-current with 1 M D2EHPA selectively extracts Mn, leaving Co in raffinate ; reports purity >99.9% for Co/Mn/Ni solutions	High-purity individual metal solutions (Co, Mn, Ni)	Shows that flowsheet staging (not single-contact only) can achieve very high purities	(Yun et al. 2024)

Mn/Co/Ni leach liquor (waste mobile-phone LIBs)	Temperature-effect SX trends (D2EHPA)	20 vol% D2EHPA in kerosene; temperature 25→55 °C. At pH 3, Mn extraction 93.4→98.3%, while Co extraction decreases (39.6→27.5%) . Example at pH 2.5 gives ~84% Mn, 8.6% Co, 6.2% Ni	Improved Mn/Co selectivity with temperature (in their tested window)	Useful as a selectivity/temperature benchmark and shows multi-step extraction–scrubbing logic	(Nadimi and Karazmoudeh 2021)
Mn recovery from LIB-recycling solutions (process/operability emphasis)	Continuous SX in column (D2EHPA)	Column operation (pulsed-disc & doughnut columns) explored; reports extraction yield >0.94 at higher pulsation intensity and suitable phase ratio	Mn recovery feasibility with hydrodynamics/operability emphasis	Highlights that industrial relevance depends on contactor hydrodynamics, not only equilibrium selectivity	(Keller et al. 2021)

Spent LIBs (aqueous)	Selective ammonia leaching + $MnCO_3$ formation	Reports high-purity $MnCO_3$ (>99.0%) with 82.1% recovery after two-stage leaching	Direct $MnCO_3$ synthesis as product	Strong example of precursor-oriented endpoint ($MnCO_3$)	(C. Wang et al. 2020)
Sulfate leach solutions (ternary cathodes)	Hybrid precipitation + SX (P507)	99.9% Al removed by phosphate precipitation; then 1 M P507 (60% saponified) with O/A=1.4, ~4 min extracts Mn/Co/Ni (reported ~90% Mn, 99% Co, 94% Ni)	Staged recovery from complex sulfate media	Good "incumbent hydromet" benchmark showing multi-step logic in mixed-cathode leachates	(Seyf and Zarei 2022)

This thesis adopts an integrated "leach → Mn-selective SX → precipitation" logic that is consistent with these literature directions but focuses explicitly on DES-derived leachates and a $MnCO_3$ precursor endpoint. The key literature implication is that selectivity and product quality depend strongly on (i) controlled feed composition (measured streams), (ii) pH control and extractant conditioning, and (iii) impurity management through scrubbing/stripping and controlled precipitation/washing (Keller et al. 2021; Nadimi and Karazmoudeh 2021; Vieceli et al. 2020; Yun et al. 2024).

2.5 Summary and Research Gaps

Overall, the literature shows that DESs can dissolve Li and transition metals from spent cathodes under moderate-to-elevated conditions, with strong potential for chemistry-led solvometallurgical flowsheets (Fan et al. 2023; Luo et al. 2022; Tang et al. 2022; Tran et al. 2019). At the same time, the field's most persistent limitations are not dissolution alone but operability (viscosity/hydration), solvent/stream management, and integrated downstream separations with defined products (Dong et al. 2023; Fan et al. 2023; Luo et al. 2022; Rautela et al. 2023; Su et al. 2024; Tang et al. 2022; Tran et al. 2019). For Mn recycling culminating in $MnCO_3$, the most relevant gaps can be summarized as follows:

- **Controlled time–temperature datasets in a defined hydration regime**

  Many studies vary multiple parameters simultaneously, making it difficult to isolate time/temperature effects under a controlled water window and it is critical for glucose-based DES systems where viscosity and speciation are hydration-sensitive (Dong et al. 2023; Hammond et al. 2023; Rozas et al. 2021).

- **Mn-selective separation from DES-derived multicomponent feeds with auditable streams**

  D2EHPA is well-established for Mn selectivity in aqueous systems, but fewer studies demonstrate robust Mn/Co/Ni selectivity starting from DES-derived feeds with defined phase behavior and measurable stream compositions (Nadimi and Karazmoudeh 2021; Su et al. 2024; Vieceli et al. 2020; Yun et al. 2024).

- **Direct precursor-oriented demonstrations ($MnCO_3$) with impurity control**

  Many reports end at dissolved metals or intermediate salts; fewer connect separation selectivity to a verified precursor product stream with defined purity metrics and practical washing/closure logic (Su et al. 2024; C. Wang et al. 2020).

- **System-level benchmarking vs incumbent routes**

  Reviews call for clearer benchmarking of DES-enabled routes against established hydrometallurgy in terms of unit operations, selectivity, solvent/reagent management, and practical operability especially for Mn pathways. (Baum et al. 2022; Martín et al. 2023; Srivastava et al. 2023; Zhu et al. 2023).

Accordingly, this thesis focuses on a water-modified ChCl:D-glucose DES to quantify time–temperature leaching behavior, then implements D2EHPA-based Mn-selective SX followed by carbonate precipitation to $MnCO_3$, emphasizing measurable streams and an integrated leach-to-precursor endpoint.

CHAPTER 3 METHODOLOGY

3.1 Overview and Experimental Workflow

This chapter consolidates the common materials, experimental procedures, analytical methods, and performance metrics used across the experimental chapters. The methodology was designed to demonstrate an Mn "leach-to-precursor" route in which a water-modified choline chloride: D-glucose deep eutectic solvent (DES) is coupled to Mn-selective solvent extraction and direct carbonate precipitation of $MnCO_3$.

Figure 3-1 presents the overall experimental framework and the key laboratory unit operations employed in this thesis. The workflow comprised: (i) safe cell discharge and manual dismantling, (ii) cathode powder recovery and pretreatment, (iii) DES synthesis and DES leaching, (iv) solid–liquid separation to obtain a clarified leachate for downstream processing, (v) Mn-selective solvent extraction (SX) using D2EHPA followed by organic washing and acid stripping, and (vi) carbonate precipitation to produce $MnCO_3$ as a solid precursor product.

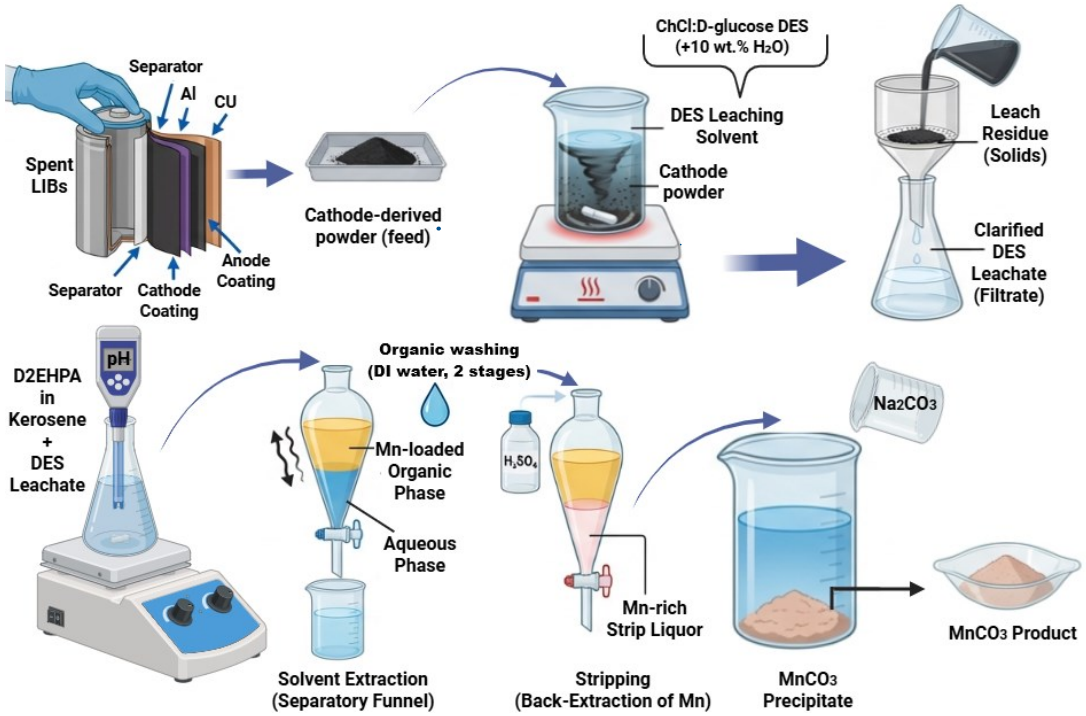

Figure 3-1. Schematic overview of the experimental workflow and key unit operations for the integrated leach → Mn-selective SX → precipitation route to $MnCO_3$ from spent LIB cathodes using a water-modified ChCl:D-glucose DES.

To support auditable performance evaluation and stage-wise mass balancing, the main process streams generated along the workflow include the clarified DES leachate (SX feed), the raffinate after extraction, the Mn-loaded organic phase, the combined strip liquor, and the washed/dried $MnCO_3$ precipitate. Detailed experimental conditions and analytical methods for each unit operation are provided in Sections 3.2–3.5, while study-specific operating envelopes are discussed in the corresponding experimental chapters.

3.2 Materials and Reagents

Two commercial cylindrical 18650 LIB types were used as cathode feedstocks: (i) MNKE IMR 18650 30A (model MH4669; nominally LiMn2O4-based, LMO-dominant) for the DES leaching parametric study, and (ii) Panasonic CGR18650CG (nominal 2250 mAh, 3.6 V; NMC-type cathode) for the integrated Mn-selective separation and product recovery study.

Choline chloride (ChCl) and D-glucose were used to prepare the DES (HBA and HBD, respectively). Di-(2-ethylhexyl) phosphoric acid (D2EHPA, ≥97%) was used as the solvent extractant and diluted in kerosene. Sodium hydroxide (NaOH) and sulfuric acid (H_2SO_4) were used for pH adjustment and partial saponification of the organic phase. Sodium carbonate (Na_2CO_3) was used as the carbonate precipitant. Hydrochloric acid (HCl) and nitric acid (HNO3) were used for acid digestion of solids and for preparation of analytical solutions. All chemicals were analytical grade and obtained from Thermo Fisher Scientific. Deionized (DI) water from an in-lab purification system was used for all experiments.

3.3 Preparation and Analysis of Cathode Materials from Spent Cells

Prior to dismantling, cells were electrically discharged in an aqueous salt solution to reduce residual voltage to a safe level (typically <2 V) and mitigate fire risk during opening and separation steps (Ojanen et al. 2018; Shaw-Stewart et al. 2019). Cells were manually dismantled to separate the cathode assembly and remove non-cathode components.

Cathode coatings were separated from the aluminum current collector by selective dissolution of aluminum in concentrated NaOH (7 M), following:

$$2Al + 2NaOH + 2H2O \rightarrow 2NaAlO2 + 3H2 \quad \text{(Eq. 3.1)}$$

After aluminum dissolution, the remaining solids were filtered and washed thoroughly with DI water. The recovered cathode powder was dried (70 °C, 24 h) and calcined (600 °C, 6 h) to remove residual organics (binder/carbonaceous species) and improve subsequent leaching operability. The calcined material was ground using a planetary ball mill (Retsch PM 200) to obtain a fine powder (<75 μm) suitable for leaching tests.

Particle size distributions of milled cathode powders were measured using a laser scattering particle size analyzer (HORIBA LA-960/LA-950 series). Measurements were performed under controlled agitation with short ultrasonic dispersion to ensure homogeneous suspension. Bulk metal content of the prepared cathode powders was determined by acid digestion followed by ICP analysis. In a representative protocol, ~0.5 g of dried powder was digested using an HNO3: HCl (1:3, v/v) acid mixture; digests were diluted to volume with water and further diluted in 1% HNO3 prior to ICP measurement.

3.4 DES Preparation and Leaching Experiments

A ChCl: D-glucose DES was prepared by mixing ChCl and D-glucose at a 2:1 molar ratio and heating at 70 °C under continuous stirring (~400 rpm) until a homogeneous liquid formed (Goudarzi et al. 2025). A water-modified formulation containing 10 wt.% water was also prepared to reduce viscosity and improve mass transfer while maintaining stable phase behavior, consistent with the known sensitivity of ChCl-based sugar DES systems to controlled hydration (Rozas et al. 2021; Seyf and Zarei 2022). The prepared DES was stored in sealed containers at room temperature prior to use.

For parametric leaching tests, 50 mg of cathode powder was contacted with 5 mL of DES in sealed glass vials (solid loading ≈10 g/L). Slurries were stirred on a hotplate stirrer (~400 rpm) at selected temperatures (60–110 °C) for contact times between 2 and 24 h. After leaching, slurries were filtered using 0.45 μm syringe filters to obtain clarified leachates for metal analysis.

For the integrated separation study, the leaching procedure was performed at the optimized condition reported previously for the water-modified ChCl:D-glucose DES (100 °C,

24 h, ~10 g/L) (Goudarzi et al. 2025). For SX experiments, the leaching step was scaled up while maintaining the same solid-to-liquid ratio; in the representative mass-balance experiment, ~0.60 g of cathode powder was contacted with ~60 mL of DES. Clarified leachate was obtained by 0.45 μm membrane filtration.

Metal leaching efficiency (η) was calculated from the dissolved metal concentration in the leachate according to:

$$\eta x\ (\%) = (Cx \cdot V / mx) \times 100 \qquad \text{(Eq. 3.2)}$$

where Cx is the concentration of metal x in the filtrate (mg L/1), V is the leachate volume (L), and mx is the initial mass of metal x present in the solid feed (mg) determined from bulk composition measurements.

3.5 Manganese Recovery via Solvent Extraction and Carbonate Precipitation

Clarified DES leachate was used as the aqueous feed for solvent extraction after adjusting the pre-contact pH to a specified setpoint using NaOH and H_2SO_4. All reported pH values refer to pre-contact pH (measured immediately before organic–aqueous contact). pH measurements were carried out using a laboratory pH meter calibrated using standard buffers (pH 4.00, 7.00, and 10.00) prior to each test series.

The organic phase was prepared by dissolving D2EHPA in kerosene to the desired extractant concentration (typically 0.6 M). Partial saponification of the organic phase was conducted using NaOH to select degrees (10–40%) to control extraction behavior and phase stability (Keller et al. 2021; Nadimi et al. 2021; Vieceli et al. 2020; Yun et al. 2024). Batch extraction tests were conducted at room temperature (25 ± 2 °C) using separatory funnels. The

aqueous and organic phases were contacted at selected organic-to-aqueous (O/A) ratios (0.5–1.5), mixed (10 min, ~500 rpm), and then allowed to disengage (≤20 min) prior to sampling.

After extraction, the Mn-loaded organic phase was washed in two stages with DI water to remove entrained DES leachate prior to stripping. In each wash, the organic phase was contacted with fresh DI water at an O/A ratio of 1:1 for 10 min under the same mixing conditions as the extraction stage.

Manganese was removed twice from the organic phase obtained after the wash step using sulfuric acid solutions. In both stages, the organic phase was extracted with fresh 1.0 M H2SO4 at an organic to aqueous ratio of 5:1 for 15 min. The combined strip liquors provided an Mn-rich sulfate solution ready for precipitation.

$MnCO_3$ was precipitated from the strip liquor by adding 1.0 M Na_2CO_3 with magnetic stirring at 400 rpm and 25 °C for 60 minutes, with the pH adjusted to the range of 8-9, thus facilitating the precipitation of $MnCO_3$ and preventing the co-precipitation of impurities (C. Wang et al. 2020). The precipitated material was filtered, washed thrice with DI water (30 mL each time), and then dried at 80 °C for 24 hours.

Aqueous concentrations of metals were determined by Inductively Coupled Plasma Mass Spectrometry (ICP-MS, Agilent 7700 series). In selected leaching experiments, the concentration of metals was determined by Atomic Absorption Spectrometry (AAS, PerkinElmer). The crystalline structure of solid materials (cathode powders and $MnCO_3$) was investigated by X-ray diffraction (XRD) with Cu Kα radiation, 2θ from 5 to 80°, step size 0.01°, and scan rate 5° /min. Functional groups of the components and solid samples were investigated by Fourier Transform Infrared Spectrometry (FTIR) from 4000 to 400 cm^{-1}. Differential

scanning calorimetry (DSC) experiments were performed to investigate the thermal properties and to support the formation of DES. Elemental composition of $MnCO_3$ products was determined by ICP analysis of acid-digested solids to quantify Mn and impurity elements (e.g., Co, Ni, Fe, Na, S).

The distribution ratio (D_M) for each metal *M* was calculated as:

$$DM = [M]org / [M]aq \quad \text{(Eq. 3.3)}$$

where $[M]_{org}$ and $[M]_{aq}$ are the metal concentrations in the organic and aqueous phases, respectively, determined after phase contact (10 min) and phase disengagement. Organic-phase metal concentrations were not measured directly; instead, they were estimated by mass balance from aqueous-phase concentrations measured before and after contact and the known phase volumes. Accordingly, distribution ratios computed using $[M]_{org}$ represent mass-balance estimates that assume complete phase disengagement and negligible phase entrainment/losses Partial saponification.

The separation factor between Mn and a competing metal M was calculated as:

$$\beta(Mn/M) = DMn / DM \quad \text{(Eq. 3.4)}$$

Accordingly, D_M and β values reported in this work represent operational values at the selected contact time, rather than independently verified thermodynamic equilibrium values.

Stripping efficiency was calculated as the fraction of metal transferred from the loaded organic phase to the aqueous strip solution relative to the initially loaded amount. The apparent precipitation recovery to $MnCO_3$ was calculated as the ratio of Mn mass measured in the washed/dried precipitate to the total Mn mass in the combined strip liquors. Because

precipitation filtrates and wash waters were not systematically analyzed, precipitation recovery is reported as an apparent recovery to the solid product.

CHAPTER 4 ENHANCED METAL RECOVERY FROM SPENT LIB USING DEEP EUTECTIC SOLVENTS

4.1 Chapter Overview

This chapter presents the results and discussion of the first experimental component, which examines deep eutectic solvent (DES) leaching of Mn-rich spent LIB cathode powder using a choline chloride–D-glucose DES. A binary DES (ChCl:D-glucose) is compared with a water-modified formulation containing 10 wt.% H_2O, and the effects of temperature and time on Li, Mn, and Ni dissolution are quantified. Leaching experiments were conducted over 60–110 °C and 2–24 h at a solid loading of ~10 g L^{-1}, followed by 0.45 μm filtration and metal analysis (AAS/ICP-based) to calculate leaching efficiencies. Experimental procedures and common analytical methods are described in chapter 3; only results-relevant details are referenced here.

4.2 Feedstock and DES Characterization

Cathode powder preparation (discharge, dismantling, Al dissolution, drying/calcination, and milling) followed the protocol described in chapter 3. Figure 4-1 summarizes the particle-size distribution of the ball-milled cathode powder. The distribution was dominated by

fine particles (clay-size), with ≈90% < 3 µm, a median size of 1.513 µm, a mean size of 1.802 µm, and a standard deviation of 1.093 µm.

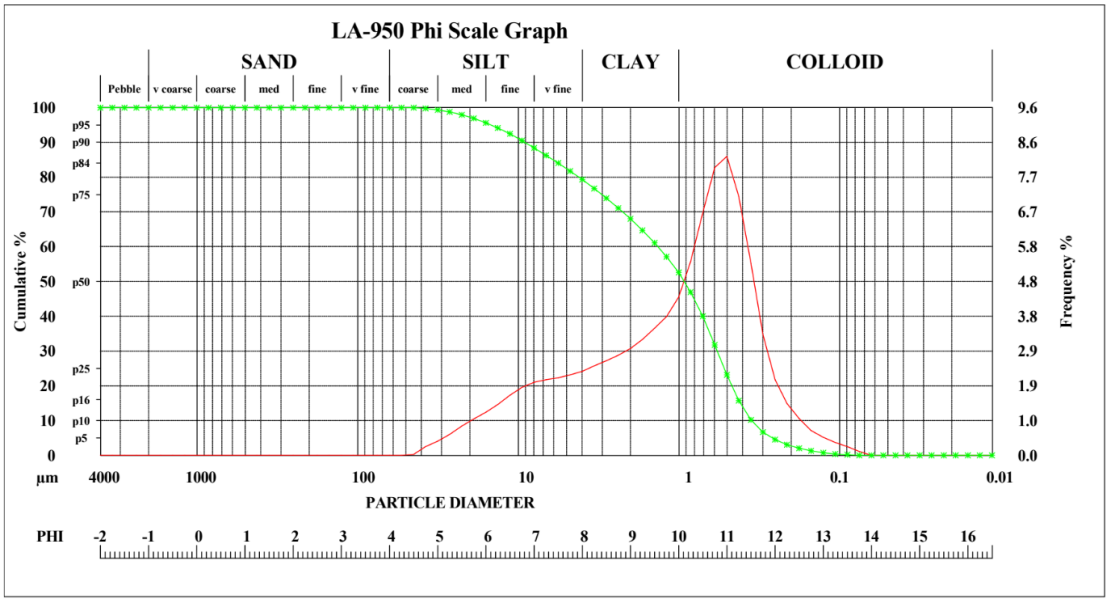

Figure 4-1. Results of particle size distribution analysis for the ball-milled cathode powder

Bulk elemental composition of the prepared cathode powder (after acid digestion) is summarized in Table 4-1. Mn was the dominant metal component, followed by Ni and Co, while Al and Cu were present at low levels, consistent with effective current-collector removal and washing.

Table 4-1. Elemental composition of cathode powder analyzed by ICP-MS

Element	Lithium (Li)	Manganese (Mn)	Nickel (Ni)	Cobalt (Co)	Aluminum (Al)	Copper (Cu)
Weight Percentage (%)	2.5	33.78	8.74	7.90	0.17	0.017

The X-ray diffraction (XRD) pattern of the active cathode material heated at 600 °C for 6 h is shown in Figure 4-2. The measured diffraction pattern exhibits major reflections at 2θ = 18.7°, 36.3°, 44.2°, 58.3°, and 64.0°, which are consistent with the (111), (311), (400), (511), and (440) planes of a spinel-type phase and show good agreement with the reference pattern of $LiMn_2O_4$ (JCPDS no. 35-0782). This overall correspondence suggests that the calcined cathode powder predominantly retains a spinel $LiMn_2O_4$-type structure after heat treatment.

It should be noted, however, that phase identification based solely on the apparent absence or presence of individual reflections may be affected by peak overlap, particularly in complex cathode materials. Therefore, the phase assignment in the present study is based primarily on the overall agreement of the diffraction pattern with the characteristic reflections of spinel $LiMn_2O_4$, rather than on the exclusion of other possible phases from individual peak positions alone. Accordingly, the XRD results support the assignment of a spinel $LiMn_2O_4$-type structure as the major crystalline component of the calcined cathode powder, while minor contributions from other phases cannot be completely excluded.

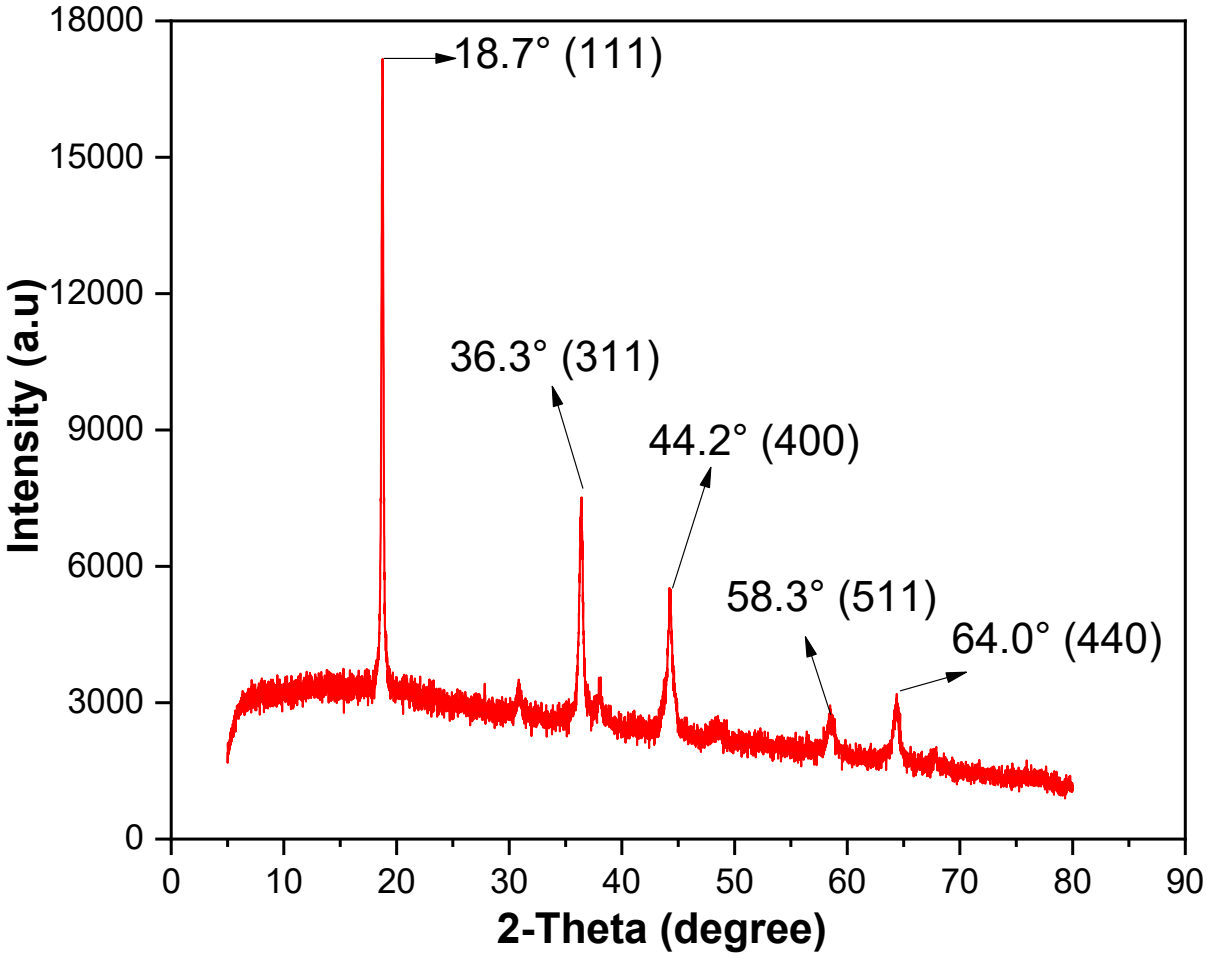

Figure 4-2. XRD pattern of the active cathode materials after heat treatment at 600 °C for 6 h

The Differential Scanning Calorimetry (DSC) results validate the effective creation of deep eutectic solvents by the notable decrease in the melting points below those of the individual components. While the melting point of the binary DES is 81.06 °C, consisting of ChCl and D-glucose, the melting point of the ternary DES, containing 10 wt.% of water, is 50.34 °C. This lowering of the melting point below that of choline chloride (302 °C) and D-glucose (146 °C) confirms the creation of the eutectic mixture, which is retained in the liquid form due to the

presence of strong hydrogen bonding forces between the components.(Abbott et al. 2004; Smith et al. 2014)

The presence of 10% water by weight of the ternary DES has a large impact on the thermal properties of the ternary DES. Water is a hydrogen bonding donor as well as a plasticizer. This leads to a decrease in intermolecular forces, causing a decrease in the melting point(Aravena et al. 2023; Gabriele et al. 2019; Kivelä et al. 2022; Meredith et al. 2024). This phenomenon is already proven in previous studies, which revealed that the addition of water increases the fluidity of DESs. This is due to the decrease in viscosity as well as an expansion of the liquid phase of DESs(Meredith et al. 2024; Rozas et al. 2021). The lower melting point of ternary DESs compared to binary systems emphasizes that water plays a crucial role in adjusting physicochemical properties of eutectic solvents.

In addition to the shift in melting points, the DSC thermograms reveal a distinct difference in peak shapes between the binary and ternary DESs. The binary DES shows a sharp, well-defined endothermic peak, indicating a relatively ordered hydrogen bonding network and a clear phase transition. In contrast, the ternary DES exhibits a broader and smoother melting peak. This can be attributed to the structural disruption caused by the presence of water, which introduces molecular disorder and increases configurational entropy. Water interferes with the organized hydrogen bonding between ChCl and glucose, resulting in a distribution of melting events over a broader temperature range. Similar broad thermal transitions in water-containing DESs have been reported in previous studies (Smith et al. 2014), supporting the view that the broadened peak reflects increased heterogeneity in the system.

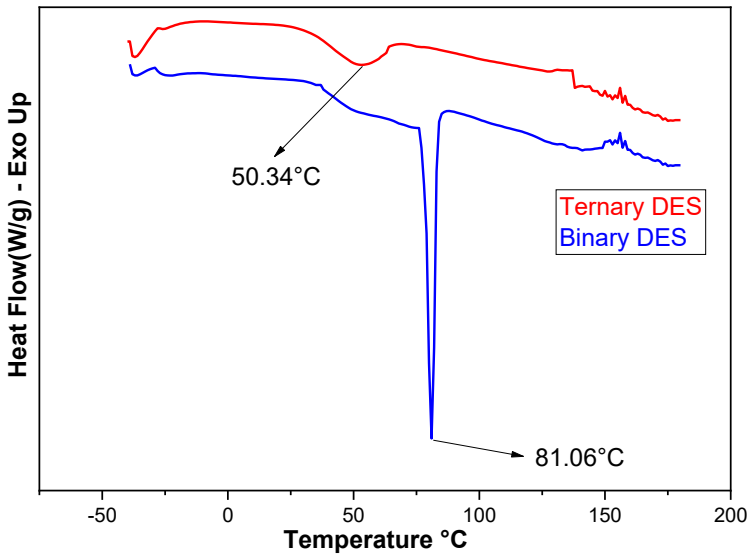

Figure 4-3. The DSC thermograms of the Ternary and Binary DES from -50 °C to 180 °C

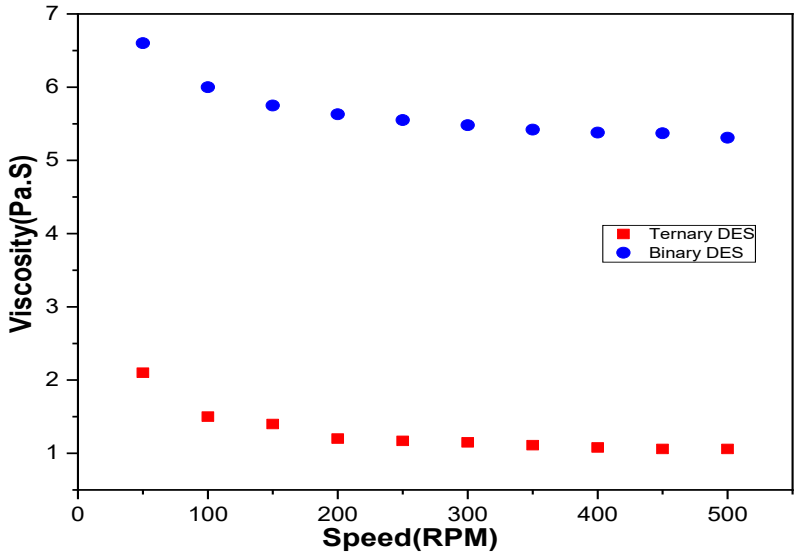

Figure 4-4. Viscosity comparison of binary and ternary DESs at room temperature.

Figure 4-4 illustrates the viscosity behavior of binary and ternary DES systems evaluated at room temperature (25 °C) across various spindle speeds ranging from 50 to 500 RPM. The binary DES, composed of choline chloride and glucose, exhibited significantly higher viscosities, starting at 6.6 Pa·s at 50 RPM and gradually decreasing to 5.31 Pa·s at

500 RPM. In contrast, the ternary DES—prepared by incorporating 10 wt.% water—showed a much lower viscosity range, from 2.1 Pa·s to 1.065 Pa·s. The consistent decrease in viscosity with increasing speed indicates pseudoplastic (shear-thinning) behavior, which is typical of DES systems. The considerable reduction in viscosity upon water addition is attributed to the disruption of the strong hydrogen bonding network between DES components. This not only reduces internal resistance and improves fluidity but also enhances mass transport and diffusion(Aravena et al. 2023; Peng et al. 2024; Seyf and Zarei 2022). Such improved dynamic properties are particularly beneficial in leaching applications, where efficient metal recovery from spent batteries depends heavily on effective solvent mobility.

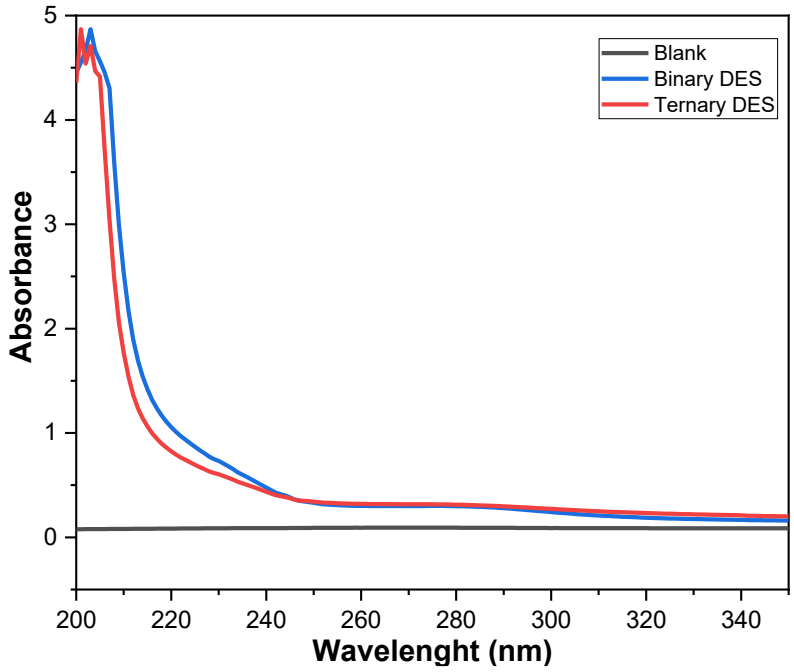

Figure 4-5. UV-Vis spectra of binary and ternary DESs between 200–400 nm

Figure 4-5 shows the UV-Vis absorption spectra of the binary and ternary DES systems, as well as the blank sample, in the wavelength range of 200 to 350 nm. The absorption spectra of the binary DES system (Choline Chloride: D-glucose) and the ternary system with the

addition of 10 wt.% water appear very similar, with a strong absorption peak below 220 nm and a sharp decrease towards zero absorption above 250 nm. The strong absorption in the deep UV region, below 220 nm, can be ascribed to the $n \rightarrow \sigma^*$ and $\pi \rightarrow \pi^*$ transitions of functional groups like hydroxyl and amines, which are prevalent in the two components of the DES system. The fact that the two absorption spectra appear very similar indicates that the addition of water, even at the concentration of 10 wt.%, does not cause significant changes in the electronic environment and the functional group interactions of the DES system. This observation, therefore, indicates that water, which affects the physical properties of the system like viscosity, does not interfere with the molecular structure and the bonding configuration that contributes to the UV absorption, and hence the system remains chemically stable for the maintenance of the leaching functionality in hydrometallurgical processes.

The FTIR spectra authenticates the successful development of DES (ChCl + D-glucose + water) based on the prominent shifts of the key peaks. The O-H stretching peak, originally at 3220 cm^{-1} for ChCl and 3198 cm^{-1} for D-glucose, shifts to 3265 cm^{-1} for DES, indicating increased hydrogen bonding between the components. Also, the C-H stretching peak shifts to 2922 cm^{-1} for DES, reflecting a change in structure due to molecular interaction. The key C-O stretching peak for glucose at 990 cm^{-1} shifts to 1028 cm^{-1} for DES, demonstrating a modification in bonding due to hydrogen bonding effects. Also, the quaternary ammonium-related peak for ChCl at 954 cm^{-1} has been maintained, confirming that the ionic character has been retained for ChCl.

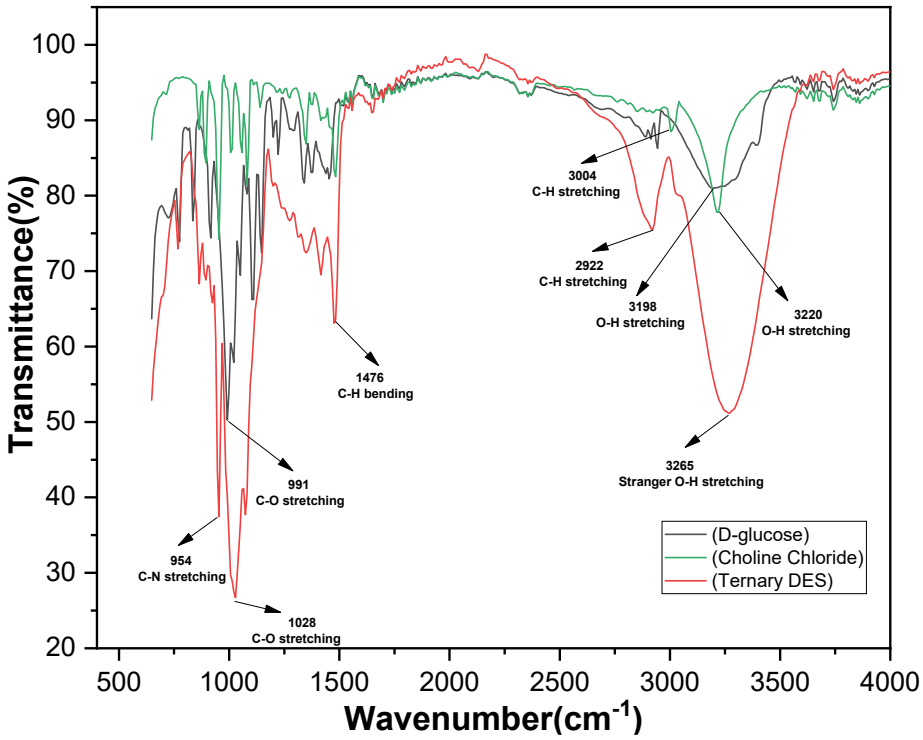

Figure 4-6. FTIR Spectra Comparing the DES with Its Individual Components (Choline Chloride and Glucose)

4.3 Leaching of spent LIB sample

4.3.1 Effect of temperature on leaching efficiency using DES

Figure 4-7 and Figure 4-8 present the comparative leaching efficiency of Li, Mn, and Ni at different temperatures (60–110 °C) using binary and ternary deep eutectic solvents (DESs). The results clearly show that the ternary DES system exhibits significantly higher leaching efficiencies for all three metals across the tested temperature range compared to the binary DES system.

In the case of the binary DES system (Figure 4-7), the leaching efficiencies of Li, Mn, and Ni increased with temperature, reaching maximum values of 88.07%, 84.23%, and 54.81%

at 110 °C, respectively. Although the melting point of the binary ChCl–glucose DES is approximately 81 °C (as confirmed by DSC analysis), Figure 4-7 includes leaching tests conducted at 60 °C to evaluate the threshold of leaching performance. At this temperature, the DES exists in a semi-solid or highly viscous state, but partial liquefaction and limited molecular mobility can occur under continuous heating and stirring. This permits partial leaching of metal elements, although with reduced efficiency. The data thus illustrate the onset of leaching capability below the melting point and support the identification of 100 °C as the optimal temperature for efficient metal extraction with this DES system. At lower temperatures (e.g., 60 °C), the extraction efficiencies were substantially lower, particularly for Ni (7.61%), which is attributed to the stronger crystal field stabilization and ionic bonding of Ni in the NMC cathode lattice structure. Similar trends have been reported in previous studies, where Ni showed lower leaching behavior due to its higher lattice energy and lower mobility compared to Li and Mn (Ma et al. 2024; Ren et al. 2024). The consistent improvement of Li and Mn leaching with temperature is in agreement with kinetic models suggesting (Aravena et al. 2023; Chen et al. 2024; Peng et al. 2024; Seyf and Zarei 2022) that higher temperatures promote diffusion and surface reaction rates in DES systems.

In contrast, the ternary DES system (Figure 4-8), modified with 10 wt.% water, demonstrated superior leaching performance at all temperature levels. The addition of water has been shown to significantly reduce the viscosity of DESs, improving ion mobility and enhancing metal dissolution kinetics. At 60 °C, Li, Mn, and Ni showed higher leaching efficiencies (23.45%, 24.53%, and 7.89%, respectively) compared to the binary DES. The efficiencies increased with temperature and reached 98.95%, 98.43%, and 71.41% for Li, Mn, and Ni, respectively, at 110 °C. However, leaching efficiency plateaued beyond 100 °C,

indicating that further increases in temperature no longer yielded proportional improvement, likely due to saturation in metal–DES complexation and changes in solvent structure at elevated temperatures, consistent with the observations of Behnajady et al. (2024).

Importantly, the ternary DES achieved >90% recovery for Li and Mn at just 90 °C, whereas the binary DES required 100 °C to reach similar extraction levels. This result underscores the higher reactivity and lower energy demand of the ternary DES, which aligns with recent findings that show aqueous-modified DESs can significantly enhance leaching rates while reducing thermal requirements(Padwal et al. 2022; Shaibuna et al. 2022; Wang et al. 2023).

Overall, these findings confirm the superiority of the ternary DES system for metal recovery from spent LIBs, due to its lower viscosity, enhanced mass transfer, and improved complexation capacity. Such systems present a promising low-energy and environmentally friendly alternative to conventional leaching methods.

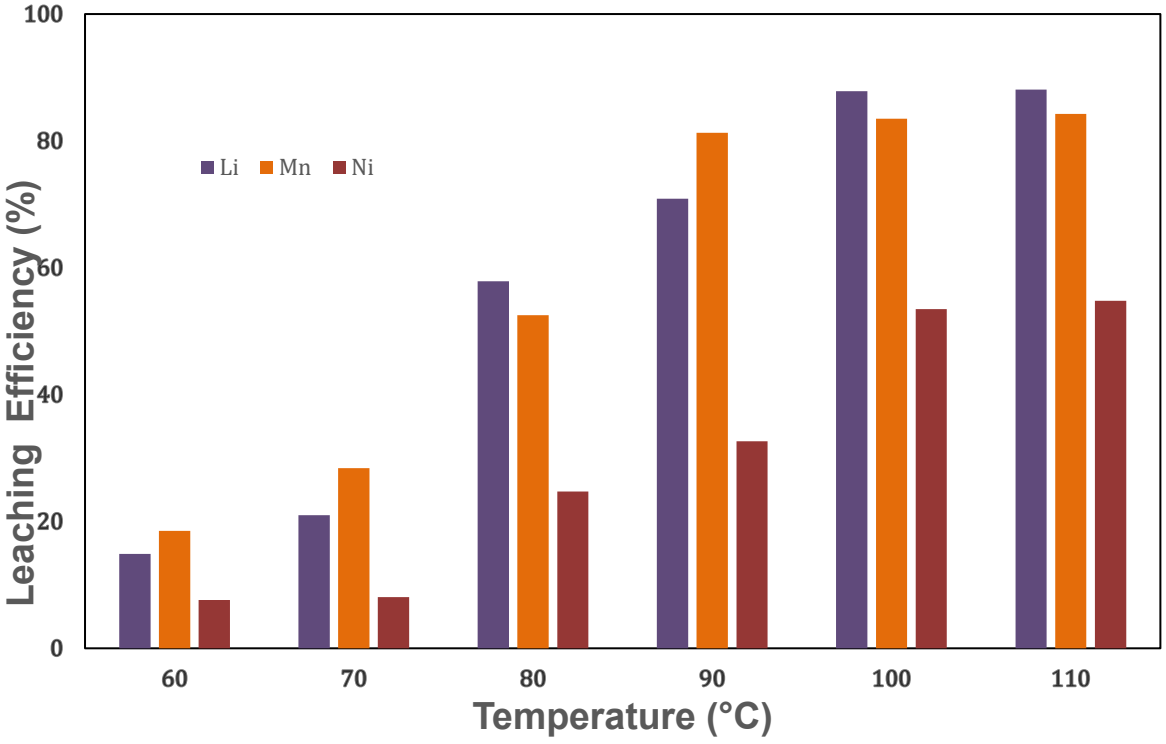

Figure 4-7. Effect of Temperature on Leaching Efficiency (Binary DES)

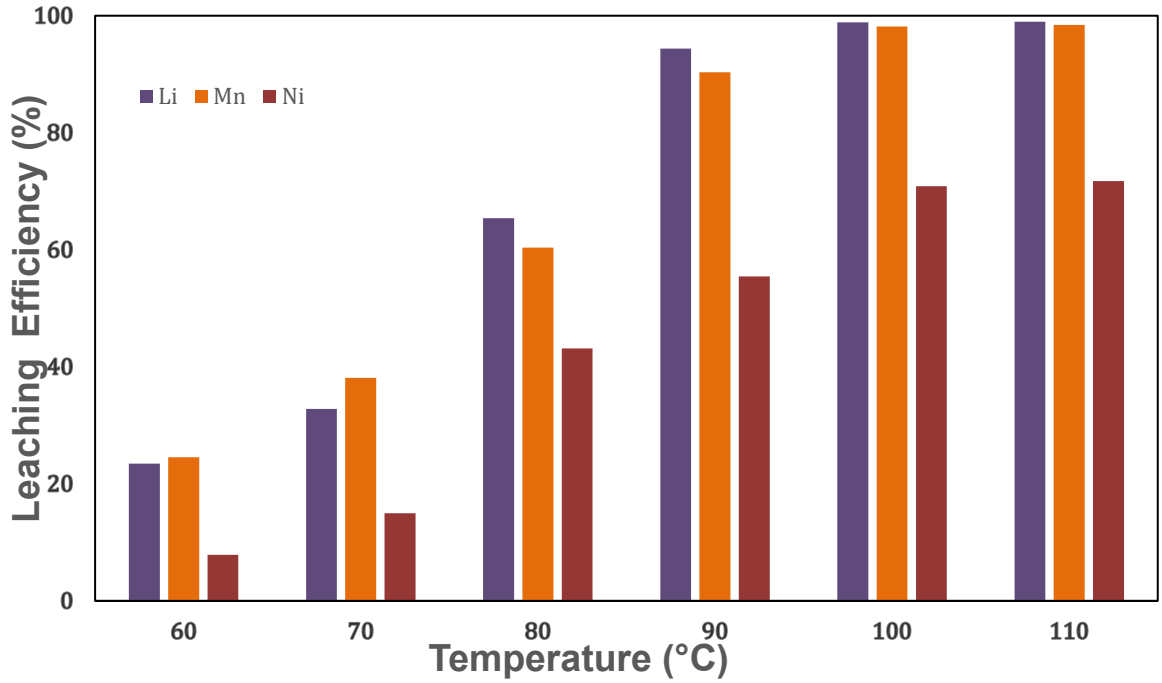

Figure 4-8. Effect of Temperature on Leaching Efficiency (Ternary DES)

4.3.2 Effect of leaching time on metal extraction efficiency using DES

Figure 4-9 illustrates the effect of leaching time at 100 °C on the extraction efficiency of Li, Mn, and Ni from spent LIB cathode material using the ternary DES system. The results demonstrate a clear time-dependent improvement in metal dissolution, with substantial increases observed as the reaction time progressed from 2 to 24 hours.

At the initial stage (2 hours), the leaching efficiencies were relatively low, with Li, Mn, and Ni reaching only 29.3%, 3.4%, and 2.0%, respectively. This suggests that the dissolution of active cathode components requires an initial activation period, during which DES components penetrate the solid matrix and begin breaking down the metal-ligand bonds(Peeters et al. 2020; S. Wang et al. 2020).

With increasing leaching duration, metal extraction efficiency showed a steady enhancement. After 12 hours, Li, Mn, and Ni reached 53.56%, 24.48%, and 12.05%, respectively, indicating that prolonged contact time significantly facilitates the diffusion and solubilization of metal ions into the DES phase.

A substantial improvement was observed after 18 hours, where Li and Mn leaching efficiencies reached 87.92% and 42.53%, while Ni extraction remained comparatively lower at 33.06%, likely due to the stronger interaction of Ni within the cathode material lattice. This trend aligns with previous studies reporting that lithium is more readily leached due to its higher mobility and weaker bonding in layered oxide structures, while Ni shows stronger bonding within the crystal lattice, making it less accessible under similar conditions(Chen et al. 2024; Zhang et al. 2021). The moderate recovery of Mn is consistent with its intermediate bonding strength and partial reduction during leaching processes. These observations suggest that

extended leaching time favors the dissolution of loosely bound metals, while more tightly bound elements like Ni may require harsher conditions or stronger complexing agents for higher recovery.

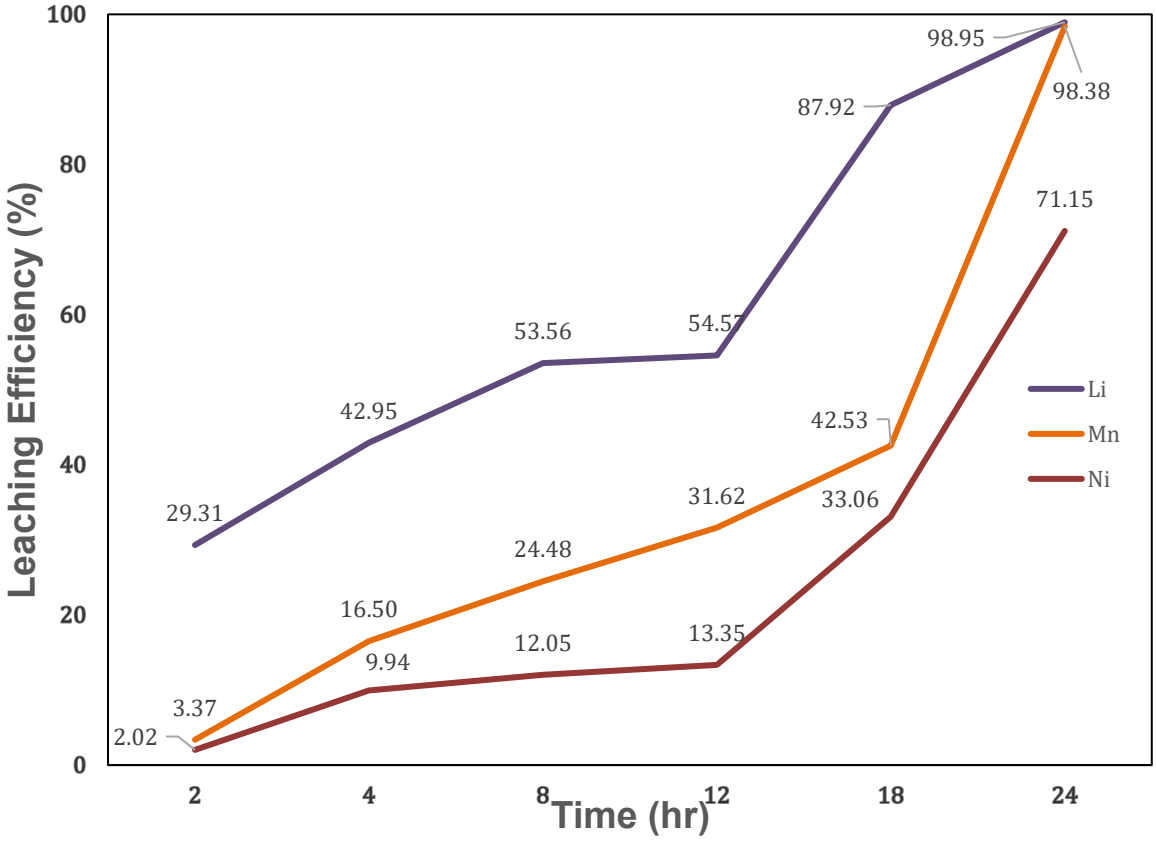

Figure 4-9. Effect of Time on Leaching Efficiency (Ternary DES)

At 24 hours, the dissolution process reached its peak, with Li, Mn, and Ni achieving 98.95%, 98.38%, and 71.15% leaching efficiency, respectively. This indicates that near-complete metal recovery is attainable with prolonged leaching, confirming the high capability of ternary DES in facilitating metal dissolution over extended durations.

These findings suggest that while shorter reaction times may not yield optimal recovery, extending the leaching duration beyond 18 hours significantly enhances efficiency, particularly

for Li and Mn. The remarkable increase in Ni dissolution at longer durations further emphasizes the necessity of prolonged reaction times for complete metal recovery.

4.3.3 Visual indicators of leaching efficiency

The color change of the deep eutectic solvent (Ternary DES) solution serves as a qualitative marker of metal dissolution, providing visual confirmation of leaching efficiency under varying experimental conditions. As shown in Figure 4-10, higher temperatures (a) and longer reaction times (b) result in progressively darker solutions, indicating increased dissolution of metal ions into the solvent. This phenomenon aligns with quantitative leaching results, demonstrating that elevated temperatures and extended durations enhance the extraction of lithium and manganese, while nickel exhibits relatively lower solubility under the same conditions. The correlation between color intensity and metal dissolution underscores the potential of DES-based leaching as an efficient and environmentally friendly approach for LIB recycling (Chang et al. 2022).

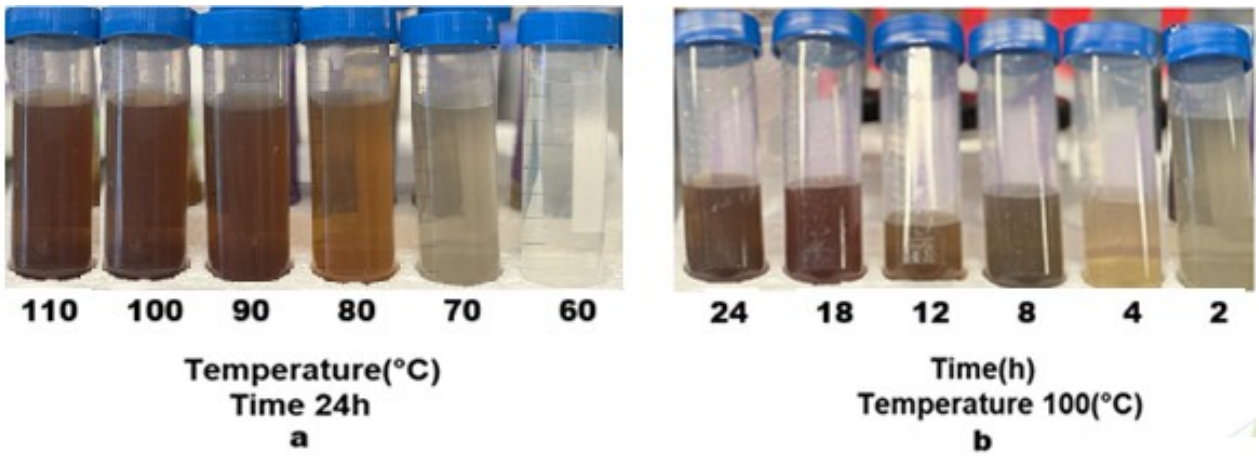

Figure 4-10. (a) Change in color of leaching solution for different temperatures over 24h. (b) Change in color of leaching solution for different times at 100(°C)

4.4 Summary

This study evaluated the effectiveness of choline chloride–D-glucose deep eutectic solvents (DESs), with emphasis on a water-modified ternary formulation, for leaching Li, Mn, and Ni from spent LIB cathode powder by systematically varying temperature and leaching duration. The data show that the ternary DES (containing 10% water) performed better than the binary DES, in agreement with the lower viscosities, improved mass transfer rates, and better dissolution of metals.

Under optimal conditions, lithium and manganese showed almost complete dissolution (>98%), although nickel dissolution was lower, which is expected due to higher lattice forces and slower dissolution/transport rates. The temperature dependence showed that the efficiencies of leaching rose with temperature but leveled off beyond 100 °C. Time-dependent tests similarly showed progressive improvements with extended leaching, with the most substantial gains occurring over approximately 18–24 h. In addition, darkening of the DES leachate provided a qualitative indicator consistent with increased dissolved-metal concentration as leaching progressed.

Overall, the findings support the feasibility of DES-based leaching as a chemistry-led alternative to conventional acid systems, while also highlighting practical constraints for scale-up, including viscosity-related operability and slower kinetics for nickel. Importantly, the optimized leaching envelope established here was adopted to generate a reproducible, multicomponent DES-derived leachate for the Mn-selective solvent extraction and $MnCO_3$ precursor production presented in chapter 5.

CHAPTER 5 SELECTIVE RECOVERY OF MN FROM DES LEACHATES OF SPENT LIBS VIA D2EHPA AND $MnCO_3$ PRECIPITATION

5.1 Chapter Overview and Study-Specific Notes

This chapter presents the results and discussion of the second experimental component, which develops an integrated leach-to-precursor route for manganese recovery from deep eutectic solvent (DES) leachates of spent lithium-ion battery (LIB) cathode materials. A multicomponent DES-derived leachate (Mn–Co–Ni–Li) was processed by Mn-selective solvent extraction (SX) using di-(2-ethylhexyl) phosphoric acid (D2EHPA), followed by washing, acid stripping, and direct carbonate precipitation to produce $MnCO_3$. Common experimental procedures and analytical methods are described in chapter 3; only results-relevant details are summarized here.

For clarity, this study used an NMC-type cathode feed and applied the same ChCl:D-glucose (10 wt.% H_2O) DES formulation and leaching envelope established in chapter 4 to generate the SX feed leachate.

5.2 Feed Characterization and Mn-Selective Solvent Extraction Performance

The DES-derived leachate was fully quantified for Mn, Co, Ni, and Li prior to solvent extraction, providing a realistic multicomponent feed for assessing Mn selectivity. Table 5.1 summarizes the initial leachate composition. This multicomponent composition is consistent with DES leaching behavior reported in the literature and with previous leaching study(Fan et al. 2023; Goudarzi et al. 2025; Wang et al. 2023).

Unlike the earlier work, in which only partial metal quantifications were possible, the present leachate contains fully quantified concentrations of Mn, Co, Ni, and Li. This provides

a realistic and chemically complex feed for evaluating selective manganese recovery by solvent extraction. The coexistence of transition metals with similar chemical properties highlights the need for a highly selective separation strategy (Keller et al. 2021; Nadimi and Karazmoudeh 2021).

Table 5-1. Chemical composition of the DES-based leachate prior to solvent extraction

Mn [mg/L]	Co [mg/L]	Ni [mg/L]	Li [mg/L]
945.6	681.4	818.3	305.4

Cation exchange was the dominant mechanism of manganese extraction from the leachate obtained from the DES into the organophosphorus extractant di-(2-ethylhexyl) phosphoric acid. The reaction of manganese (II) from the aqueous phase into the solvent extractant in the organophosphorus extractant D2EHPA can be expressed as in Equation (5.1) (Dorella and Mansur 2007; Keller et al. 2021; Lei et al. 2022; Nadimi and Karazmoudeh 2021).

$$Mn^{2+}(aq) + 2(HR)(org) \rightarrow MnR_2(org) + 2H^+(aq) \quad \text{(Eq. 5.1)}$$

where HRdenotes the acidic form of D2EHPA in the organic phase.

This mechanism explains the strong dependence of Mn extraction on the pre-contact pH and the degree of extractant saponification. Increasing pH and partially neutralizing D2EHPA reduce proton competition and increase the availability of deprotonated extractant species, which promotes Mn–D2EHPA complex formation and increases Mn loading. Because Co^{2+} and Ni^{2+} typically require higher pH (or stronger deprotonation) to be extracted to the same extent, an intermediate pH window can provide enhanced Mn/Co and Mn/Ni discrimination in

multicomponent leachates, consistent with the selectivity trends observed in this work (Dorella and Mansur 2007; Keller et al. 2021; Lei et al. 2022; Nadimi and Karazmoudeh 2021).

Based on the selected operating conditions, a stage-wise mass balance was established across extraction, stripping, and precipitation to evaluate overall process performance. The extraction step achieved the highest Mn removal from the leachate, followed by efficient stripping and precipitation, resulting in an overall Mn recovery of 81.0%. This mass balance confirms the effectiveness of the developed solvent-extraction-based route for selective Mn recovery from the DES leachate (Lei et al. 2022).

Table 5-2. Stage-wise mass balance of manganese (Mn) during the extraction, stripping, and precipitation process from battery leachate, showing input, recovered, and lost Mn, along with recovery efficiencies

Stage / Step	Mn input (mg)	Mn recovered (mg)	Recovery (%)	Mn lost (mg)
Extraction	56.74	50.87	89.7	5.87
Stripping	50.87	48.25	94.8	2.62
Precipitation	48.25	45.94	95.3	2.31
Total	56.74	45.94	81.0	10.80

Note: Precipitation recovery is reported as an apparent recovery to the recovered $MnCO_3$ solid based on ICP-MS analysis after digestion. The precipitation filtrate and wash waters were not analyzed; therefore, “Mn lost” includes Mn remaining in solution as well as handling losses.

Effect of pre-contact pH

The main controlling factor for both manganese extraction and selectivity were the pre-contact pH in the D2EHPA system. It was observed, as shown in Figure 5-1, that the extraction of Mn increased from 72.4% to 91.2% as the pH was raised from 2.1 to 3.0. This can be explained based on the cation exchange process of D2EHPA, in which the deprotonation of the extractant increases with an increase in pH (Dorella and Mansur 2007; Keller et al. 2021; Lei et al. 2022; Nadimi and Karazmoudeh 2021).

Selectivity did not improve monotonically with pH, however. Although the Mn recoveries had a maximum at pH 3.0, the separation factors had maxima at pH 2.7. At this pH, the separation factor values of $\log_{10}\beta Mn/Co = 2.16$ and $\log_{10}\beta Mn/Ni = 2.32$ correspond to $\beta Mn/Co = 143$ and $\beta Mn/Ni = 208$, respectively, representing very high extraction selectivity for Mn over Co and Ni. For pH values higher than 2.7, the reduction in $\log_{10}\beta$ with increasing pH implies higher co-extraction of Co^{2+} and Ni^{2+} ions as the deprotonated D2EHPA becomes

increasingly reactive towards the ions. The Li extraction remains too low (<1.5%) over the entire range of pH values tested and clearly reflects the very high selectivity against Li^+ ions.

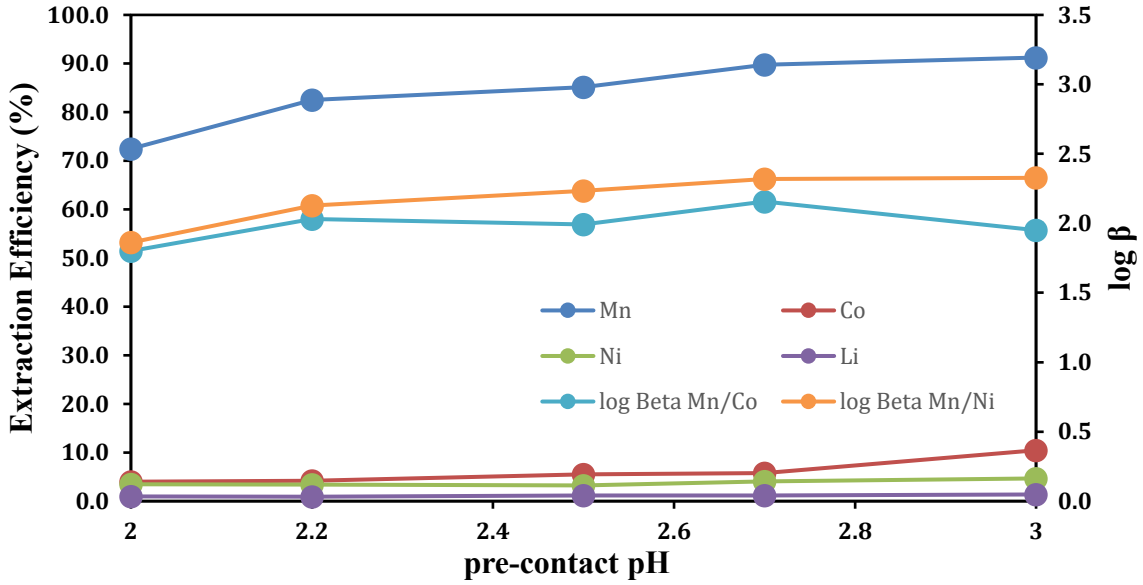

Figure 5-1. Effect of pre-contact pH on metal extraction and separation factors ($log_{10}\beta Mn/M$). Conditions: 0.6 M D2EHPA, saponification = 25%, O/A = 1:1, 25 °C.

Effect of Saponification Degree

Partial saponification was used to reduce the pH drop during extraction and to improve Mn loading. As shown in Figure 5-2, increasing the saponification degree from 5% to 25% increased Mn extraction and improved selectivity relative to Co and Ni. The highest selectivity was obtained at 25% saponification, where the $log_{10}\beta$ values reached their maximum (Dorella and Mansur 2007; Keller et al. 2021; Lei et al. 2022; Nadimi and Karazmoudeh 2021).

Further increasing saponification to 40% reduced selectivity. At high saponification levels, the organic phase becomes highly reactive, which promotes co-extraction of Co and Ni. This is why there is a corresponding decrease in $log_{10}\beta$ for 40% saponification in Figure 5-2.

Hence, 25% saponification is more optimal in achieving good Mn recovery and minimizing impurity extraction, resulting in a more preferable loaded organic fraction for subsequent washing and stripping stages.

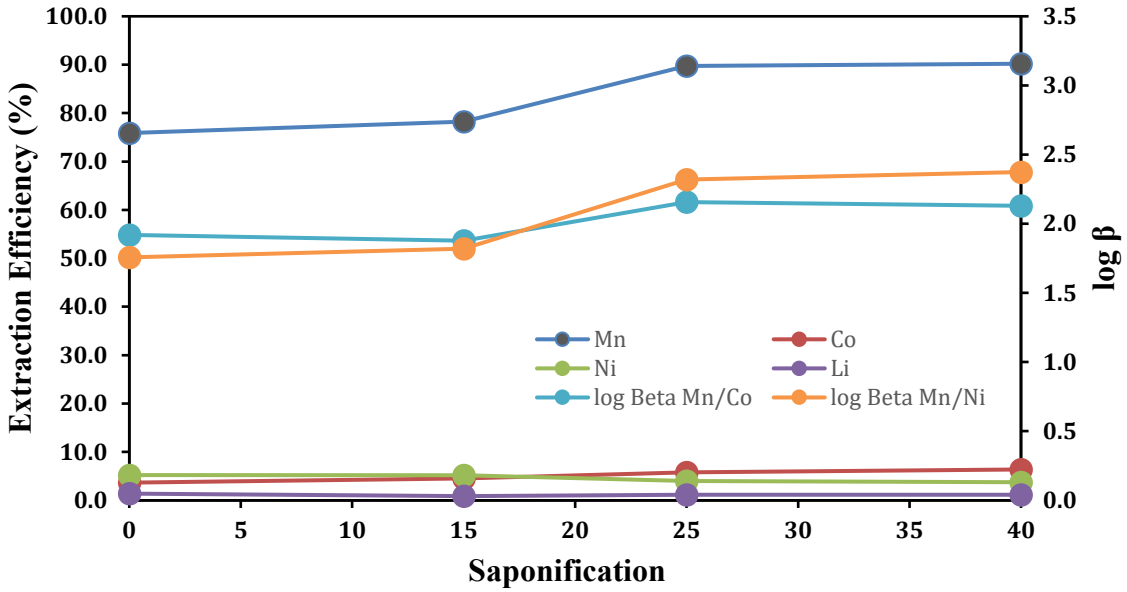

Figure 5-2. Effect of saponification degree on Mn recovery and selectivity. Conditions: pre-contact pH = 2.7, O/A = 1:1, 25 °C.

Effect of Organic-to-Aqueous Phase Ratio (O/A)

The ratio of organic to aqueous phases was then varied between 0.5 and 1.5 to find the minimum solvent requirement possible while sustaining high Mn recovery and selectivity. With a ratio of O/A = 0.5, the organic phase was close to saturation, with a noticeable amount of Mn remaining in the raffinate phase. Increasing the ratio to O/A = 1.0 provided sufficient extractant

capacity and increased Mn extraction to 89.7% (Dorella and Mansur 2007; Keller et al. 2021; Lei et al. 2022; Nadimi and Karazmoudeh 2021).

A further increase to O/A = 1.5 produced only a small gain in Mn recovery. In addition, Figure 5-3 shows a slight decrease in $\log_{10}\beta$ at O/A = 1.5, which is attributed to dilution effects and/or increased co-extraction as more extractant is available. From a practical perspective, O/A = 1.0 is preferred because it provides high Mn recovery and strong selectivity while minimizing solvent consumption and maintaining a higher Mn concentration in the loaded organic phase for the stripping stage.

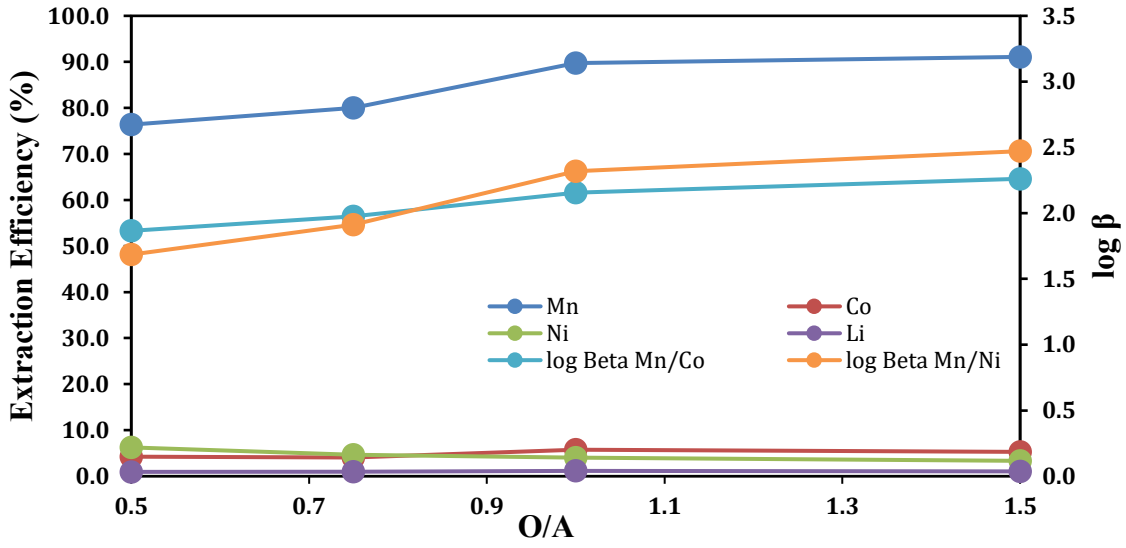

Figure 5-3. Influence of the organic-to-aqueous (O/A) phase ratio on manganese extraction efficiency and separation factors from the DES-leachate (Conditions: pre-contact pH = 2.7, Saponification = 25%, Temp = 25 °C).

5.3 Stripping and Carbonate Precipitation of Manganese

Manganese stripping from the loaded organic phase proceeds through the proton-driven dissociation of the Mn–D2EHPA complex. Upon contact with sulfuric acid, increased proton activity promotes dissociation (decomplexation) of the Mn–D2EHPA complex, regenerating the extractant and transferring Mn^{2+} to the aqueous phase, as expressed by Equation (5.2):

$$MnR_2(org) + 2H^+(aq) \rightarrow Mn^{2+}(aq) + 2HR(org) \quad \text{(Eq. 5.2)}$$

This reversibility enables efficient Mn transfer from the organic to aqueous phase and produces a $MnSO_4$-rich strip liquor suitable for carbonate precipitation. In the present work, most manganese recovered during the first stripping stage (77.4%), followed by an additional 17.4% in the second stage, resulting in a total stripping recovery of 94.8%. This staged behavior is consistent with the strong dependence of Mn stripping on acid-driven decomplexation in cation-exchange organophosphorus systems and supports the selection of two stripping stages to maximize Mn recovery while maintaining a concentrated strip liquor for the subsequent precipitation step (Dorella and Mansur 2007; Kang et al. 2010).

Following stripping, manganese was converted to $MnCO_3$ by controlled carbonate precipitation. Addition of carbonate ions promotes formation of insoluble rhodochrosite according to Equation (5.3):

$$Mn^{2+}(aq) + CO_3^{2-}(aq) \rightarrow MnCO_3(s) \quad \text{(Eq. 5.3)}$$

Precipitation was conducted at pH 7–8 and 25 °C for 60 min to favor $MnCO_3$ formation while limiting co-precipitation of other transition metals under the applied conditions (C. Wang et al. 2020). The precipitate was filtered, washed, dried, and analyzed after acid digestion by ICP. Based on Mn quantified in the recovered solid relative to Mn in the combined strip liquors

(stages 1 and 2), the apparent precipitation recovery to the recovered $MnCO_3$ solid reached 95.3%. As the precipitation filtrate and wash waters were not analyzed, this recovery represents Mn captured in the recovered solid product rather than solution depletion. Nevertheless, the high apparent recovery and the subsequent phase identification demonstrate that carbonate precipitation provides an effective final step to convert stripped Mn solutions to $MnCO_3$ under mild conditions.

5.4 Structural Characterization of Precipitated $MnCO_3$

5.4.1 X-ray diffraction (XRD) analysis

The XRD patterns of the precipitated $MnCO_3$ product closely match those of rhodochrosite (space group R-3c), with the principal reflections observed at $2\theta \approx 24.1°$ (012), 31.3–31.5° (104, strongest), 37.3–37.5° (113), 41.2–41.4° (202), and 45.0–45.8° (018). Small shifts in peak positions ($\Delta 2\theta \approx 0.08$–$0.35°$) and slight peak broadening may be associated with microstrain and crystallite-size effects arising from precipitation from a complex leachate-derived solution. A faint additional reflection is also observed at $2\theta \approx 49.6°$ ($\leq$5% of the maximum intensity), which is not readily attributable to rhodochrosite. Its low intensity suggests only a trace contribution; however, it may indicate a minor secondary phase, such as Na_2SO_4 or a residual carbonate phase. Although this feature appears negligible in amount, it cannot be conclusively assigned based on XRD alone. Therefore, further identification by Rietveld refinement and complementary characterization techniques such as SEM-EDS is recommended in future work. Accordingly, based on XRD, the recovered solid is described as predominantly rhodochrosite $MnCO_3$. Verification of chemical purity (e.g., residual Co/Ni/Fe/Na) and identification of any trace phase(s) require complementary analyses such as

ICP-MS of the digested solid and, if needed, database matching and additional characterization(C. Wang et al. 2020).

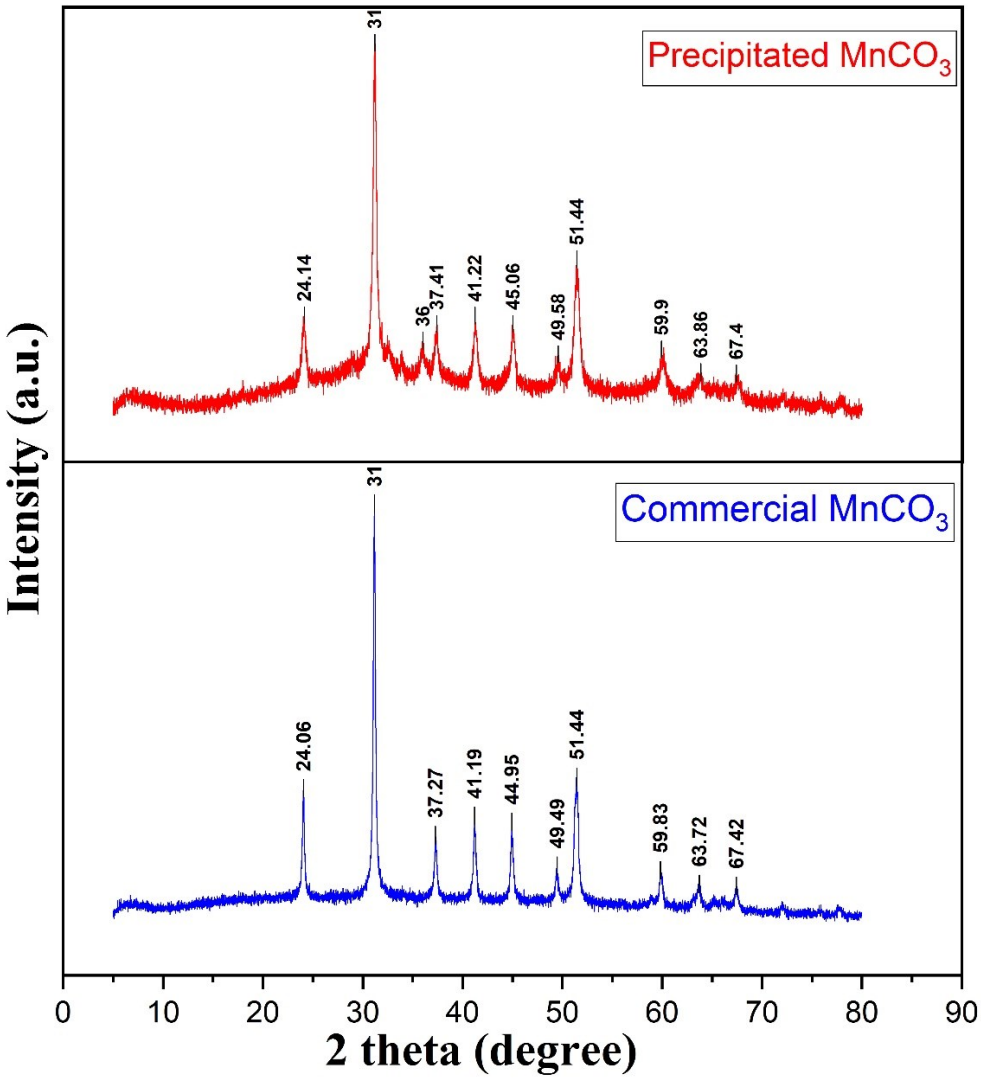

Figure 5-4. XRD patterns of $MnCO_3$ precipitated in this work (top) compared with a commercial $MnCO_3$ reference (bottom), confirming formation of crystalline rhodochrosite $MnCO_3$ (R-3c).

5.4.2 Fourier transform infrared (FTIR) analysis

The FTIR spectra of the commercial $MnCO_3$ (blue curve) and the process-derived $MnCO_3$ (red curve) collected in the range 500–4500 cm^{-1} exhibit the characteristic carbonate

(CO_3^{2-}) vibrational modes. In accordance with standard carbonate assignments, the in-plane bending mode (ν_4) appears at ~723 cm^{-1}, while the out-of-plane bending mode (ν_2) is observed at ~864 cm^{-1}. The strong band centered in the 1384–1424 cm^{-1} region corresponds to the asymmetric stretching mode (ν_3) of CO_3^{2-}. A weaker band in the 1064–1073 cm^{-1} range is attributed to the symmetric stretching mode (ν_1), which can become IR-active due to local symmetry lowering and/or structural disorder in the carbonate lattice. Lattice vibrations involving Mn–O and carbonate framework motions are expected predominantly at lower wavenumbers (notably below ~600 cm^{-1}) (C. Wang et al. 2020).

Both spectra show very similar peak positions and intensities for the fundamental carbonate bands, supporting that the precipitated product is compositionally consistent with $MnCO_3$. No prominent bands attributable to sulfate (e.g., S–O stretching), nitrate, or major organic functional groups were observed within the detectable sensitivity of FTIR in the measured range, suggesting the absence of substantial amounts of these contaminants. Broadening in the 3324–3500 cm^{-1} region can be associated with adsorbed moisture/surface hydroxylation, and weak features near ~2930 cm^{-1} may arise from trace C–H stretching. Bands around ~2117–2350 cm^{-1} can be assigned to atmospheric CO_2 and/or overtone/combination features. Overall, the FTIR results corroborate the XRD findings that the recovered solid is

consistent with $MnCO_3$, while definitive assessment of trace impurities should rely on complementary chemical analysis (C. Wang et al. 2020).

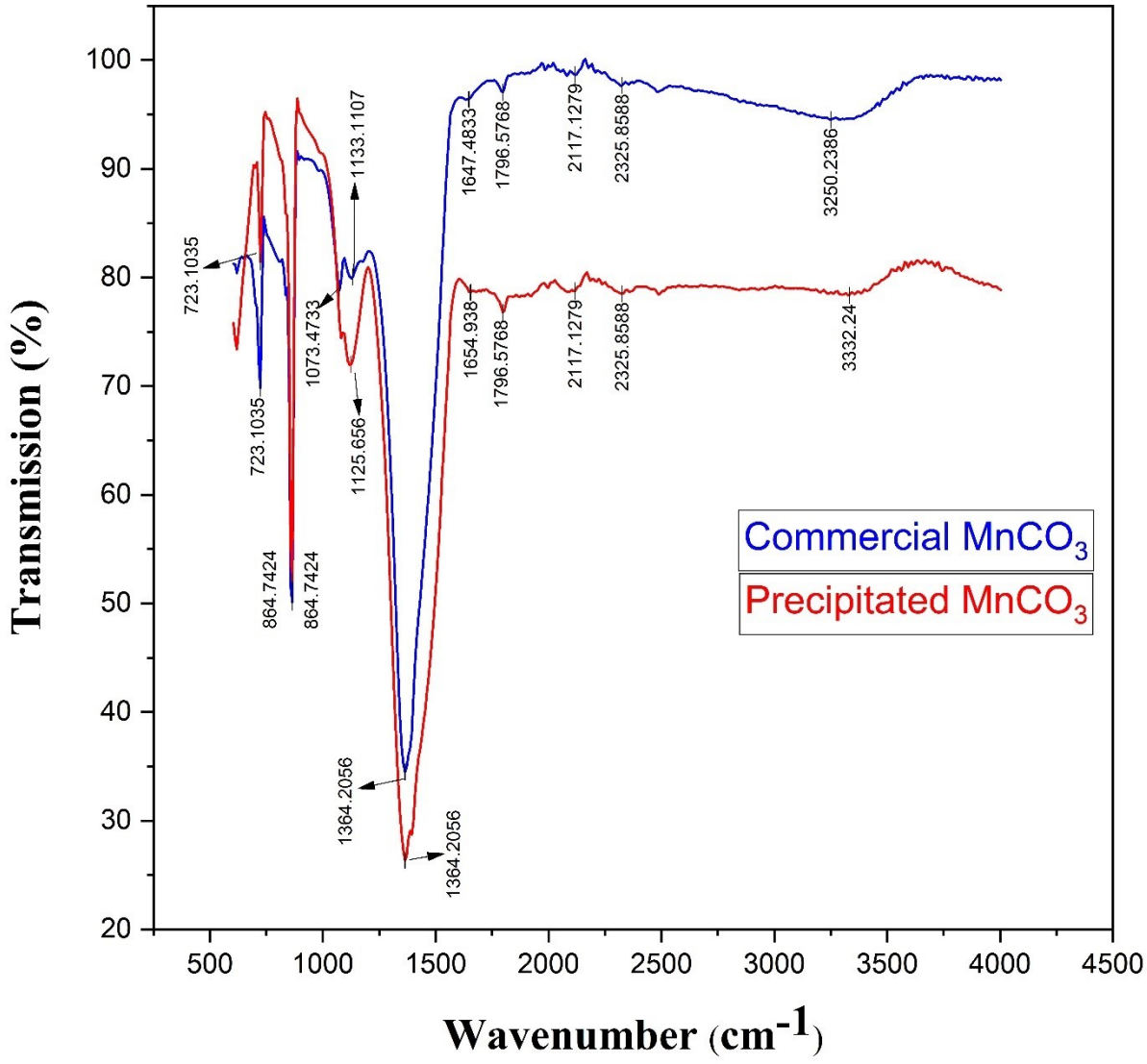

Figure 5-5. Comparison of FTIR spectra for commercial and process-derived $MnCO_3$

5.5 Comparative Analysis and Process Integration

The following comparison focuses on how the achieved selectivity and the integrated leach-to-precursor route benchmark against literature. A comparative analysis of Mn extraction performance and separation factors (β) achieved in this work versus representative literature benchmarks is summarized in

Table 5-3 and Figure 5-6. Using a ChCl:D-glucose DES-derived leachate as the extraction feed, Mn extraction of 89.7% was obtained at pre-contact pH 2.7 with 0.6 M D2EHPA (partially saponified). Under these conditions, limited co-extraction of Co, Ni and Li was observed (5.8%, 4% and 1.2%, respectively), corresponding to high separation factors of $\beta Mn/Co = 143$, $\beta Mn/Ni = 208$ and $\beta Mn/Li = 748$ ($\log_{10}\beta Mn/Co = 2.16$, $\log_{10}\beta Mn/Ni = 2.32$, $\log_{10}\beta Mn/Li = 2.87$).

As shown in Figure 5-6, these selectivity values are higher than those reported for some sulfate-leachate systems operated under their respective conditions. Although higher selectivity has been reported in some cases, these outcomes are often associated with more intensive operating strategies such as higher saponification degrees and/or different contacting configurations (e.g., column or multi-stage designs). Therefore, the main contribution of the present work is not only the selectivity level, but the integration of DES leaching with Mn-selective D2EHPA extraction and direct carbonate precipitation, enabling a concise leach-to-precursor pathway to $MnCO_3$ with limited intermediate purification steps (Dorella and Mansur 2007; Kang et al. 2010; Keller et al. 2021; Vieceli et al. 2020; C. Wang et al. 2020; Wang et al. 2023).

Table 5-3. Comparative performance and separation factors (β) of the proposed integrated DES-SX process versus established literature benchmarks using D2EHPA.

Leaching System	Extractant (conditions)	Conditions	Extraction (%)				β			Log10 βMn/Co	Log10 βMn/Ni	Log10 βMn/Li	Ref.
			Mn	Co	Ni	Li	Mn/C	Mn/Ni	Mn/Li				
DES (ChCl:D-glucose)	0.6 M D2EHPA (partially saponified)	pH 2.7	89.7	5.8	4.0	1.2	143	208	748	2.16	2.32	2.87	This Work
Synthetic NMC	D2EHPA in pulsed column	pH 2.7, O/A 1.2	84.0	~4	~2	n.r.	19.3	90.4	n.r.	1.29	1.96	n.r.	(Keller et al. 2021)
Real NMC111 Leachate	0.7 M D2EHPA (Isopar L)	pH 3.1, O/A 1.0	85	7	2	5	75.3	277.7	107.7	1.9	2.4	2.0	(Locati et al. 2024)
Waste Mobile LIBs	0.6 M D2EHPA	pH 2.5, O/A 1.0	84.0	8.6	6.2	n.r.	55.4	80.0	n.r.	1.74	1.90	n.r.	(Nadimi and Karazmoudeh 2021)
H_2SO_4–H_2O_2 leachate (spent LIB active material; NaOH impurity-precipitation)	100 g/L D2EHPA + 5 vol % TBP (Isopar L), saponified	Two-stage, SD=40% (stage1) + 20% (stage2); phase ratio=2.33; initial pH≈2.8	98.70	35.50	10.00	29.00	137.9	683.3	185.9	2.140	2.834	2.269	(Keller, Hlawitschka, and Bart 2022)
Simulated LIB sulfate leachate (Li–Ni–Co–Mn in H_2SO_4)	0.8 M D2EHPA + 5 vol % TBP (Exxsol D80)	3-stage counter-current Mn extraction, pHavg≈2.08–2.52; S/F=0.8; T=21°C	94.44	3.09	1.65	6.84	533.8	1014.3	231.6	2.727	3.006	2.365	(Jantunen, Virolainen, and Sainio 2022)

Note: β values were calculated/reported as βMn/M = DMn/DM from the cited studies; "n.r." indicates not reported. Differences in feed matrix (DES vs sulfate leachate), contactor type (batch vs column), and operating strategy (e.g., saponification degree, stage configuration) should be considered when comparing selectivity.

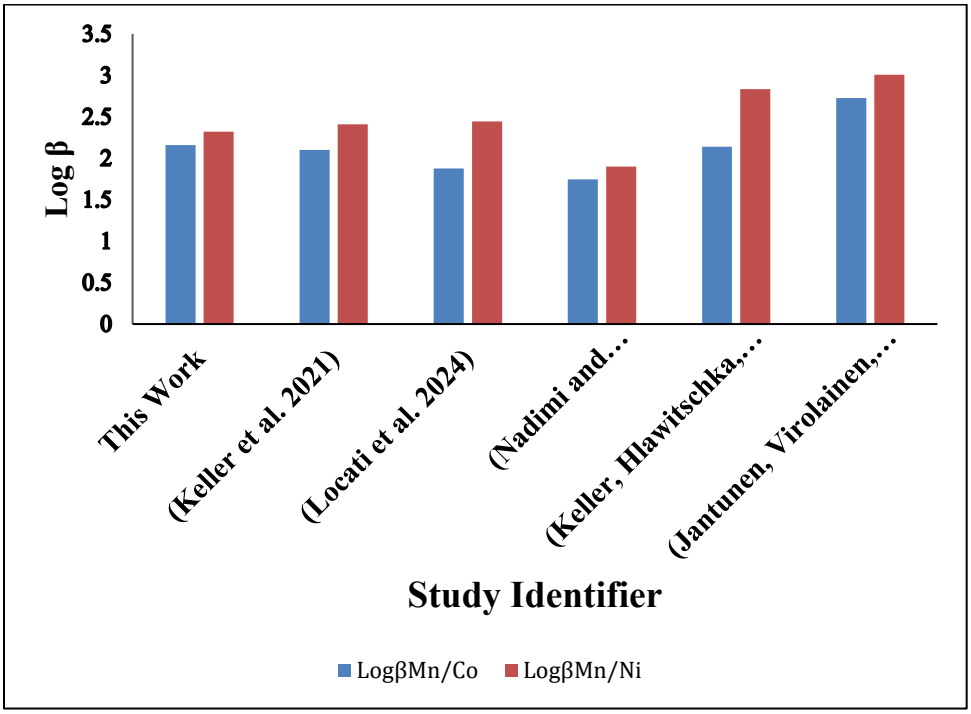

Figure 5-6. Comparison of log10(βMn/Co) and log10(βMn/Ni) values between this work and representative literature studies using D2EHPA under their reported conditions

Specifically, this study delivers $MnCO_3$ as a precursor product through an integrated, single-pass batch sequence (seeFigure 3-1): DES leaching → solid–liquid separation (filtration) → pre-contact pH adjustment of the clarified leachate → D2EHPA extraction (mixing + phase disengagement) → organic washing (mixing + phase disengagement) → two-stage acid stripping (each stage: mixing + phase disengagement) → carbonate precipitation (followed by solid–liquid separation and drying). Recycle loops (e.g., recycle of stripped organic to extraction) were not evaluated in this work and are identified as future work for continuous counter-current implementation.

The current study is limited to batch separatory-funnel experiments; therefore, industrial-scale relevance (e.g., stage requirements, phase disengagement behavior, third-phase risk, and counter-current validation) has not yet been demonstrated. Likewise, because precipitation filtrate and wash waters were not analyzed, precipitation performance is reported as an apparent recovery to the recovered solid product. Future work should (i) quantify Mn and impurities across all aqueous streams (including filtrate and washes) to provide an auditable stream table with closure, (ii) determine extraction/stripping isotherms and stage requirements for counter-current operation, and (iii) evaluate operability and sustainability metrics such as multi-cycle reuse of DES and organic phases and solvent losses, which are increasingly expected in green recycling studies (Lei et al. 2022; Su et al. 2024; Zhu et al. 2023).

5.6 Summary

This chapter demonstrates an integrated leach-to-precursor route for selective Mn recovery from a DES-derived multicomponent leachate of spent LIB cathodes. Under optimized batch conditions (0.6 M D2EHPA, 25% saponification, pre-contact pH 2.7, O/A = 1), Mn extraction reached 89.7% while Co and Ni co-extraction remained limited (≈4–6% and 3–5%), corresponding to high separation factors (βMn/Co = 143 and βMn/Ni = 208). Two-stage acid stripping recovered 94.8% of Mn from the loaded organic phase, and carbonate precipitation yielded $MnCO_3$ with an apparent recovery of 95.3%, giving an overall Mn recovery of 81.0% to the solid product. The precipitate was confirmed as rhodochrosite $MnCO_3$ by XRD and FTIR, and ICP-based digestion analysis enables quantitative assessment of elemental purity. Overall, the coupled DES–SX–precipitation sequence advances beyond dissolution to a verified $MnCO_3$ precursor stream and provides the experimental basis for the broader benchmarking and operability/scale-up discussion in chapter 6.

CHAPTER 6 DISCUSSION

6.1 Extraction and Selective Recovery of Mn from Used Batteries

Chapters 4 and 5 present two linked experimental studies: (i) leaching of an Mn-rich cathode powder using a water-modified deep eutectic solvent (DES) to define a workable dissolution envelope, and (ii) selective recovery of Mn from the resulting multicomponent leachate using D2EHPA solvent extraction (SX), followed by acid stripping and carbonate precipitation to $MnCO_3$. The purpose of this chapter is to connect the results across these steps and to explain, using the present data, why certain operating choices led to better recovery, selectivity, and operabilityThe DES background and the motivation for integrating leaching with separations are already developed in chapter 2. To avoid repeating that review, the discussion here stays close to what this thesis measured: (a) the practical operating windows that emerged from the batch experiments, (b) how the output of one unit operation constrained the next, and (c) what additional tests are needed before the same logic can be translated to staged and continuous operation.

Table 6-1. Summary of key operating windows and performance metrics across the integrated DES–SX–precipitation route.

Process stage	Key operating window (this thesis)	Key outcome / metric
DES leaching (Chapter 4)	ChCl:D-glucose (2:1) with 10 wt.% H_2O; 60–110 °C; 2–24 h; ~10 g L^{-1}	Near-complete Li and Mn dissolution (>98%) under optimized time–temperature; Ni lower (~71%)
SX optimization (Chapter 5)	0.6 M D2EHPA; ~25% saponification; pre-contact pH ≈2.7; O/A ≈ 1	Mn extraction 89.7% with limited Co/Ni co-extraction (~4–6% / 3–5%); βMn/Co = 143; βMn/Ni = 208
Organic washing + acid stripping	Two stripping contacts with H_2SO_4 (batch); staged operation	Mn stripping 94.8% producing Mn-rich strip liquor
Carbonate precipitation	Na_2CO_3; pH 7–8; 25 °C; 60 min; washed/dried solid	Apparent $MnCO_3$ precipitation recovery 95.3%; overall Mn recovery 81.0%
Product verification	XRD + FTIR; ICP digestion for composition	Rhodochrosite $MnCO_3$ confirmed; product quality quantifiable by ICP

Table 6-1 summarizes the key quantitative milestones across the integrated route demonstrated in this thesis. A simple but important message from these results is that overall performance is controlled by a small number of coupled windows, not by one "best" setting in a single unit operation. The hydration-controlled leaching conditions that gave high Li/Mn dissolution also produced a reproducible liquor that could be clarified and adjusted to a controlled pre-contact pH for D2EHPA extraction. Likewise the Mn/Co/Ni discrimination arises from operating within a narrow pH–saponification window characteristic of cation-exchange organophosphorus systems (Keller et al. 2021; Nadimi and Karazmoudeh 2021; Vieceli et al. 2020; Yun et al. 2024), while water-driven changes to DES viscosity/speciation can influence both dissolution kinetics and downstream phase behavior (Dong et al. 2023; Hammond et al. 2023; Rozas et al. 2021). These linkages are the basis for the interpretation in Sections 6.2–6.4.

6.2 Integration of Leaching Performance and Downstream Compatibility

A key practical outcome from chapter 4 is that adding 10 wt.% water to the ChCl:D-glucose DES improved handling and mixing relative to the binary DES. In day-to-day laboratory operation, this mattered because it reduced the effort needed to keep the slurry mobile and helped maintain consistent solid–liquid contact from run to run. The solvent-property basis for this behavior (viscosity and hydration effects) is discussed in chapter 2 (Section 2.3); here the focus is on what the present leaching data show (Aravena et al. 2023; Gabriele et al. 2019; Hammond et al. 2023; Peng et al. 2024).

Within the investigated time–temperature domain (60–110 °C, 2–24 h, ~10 g L^{-1}), Li and Mn dissolution approached completion (>98%) under the optimized conditions, while Ni dissolution remained lower (≈71%). This difference is important when defining a

practical operating window. For an Mn-forward circuit, the leaching step is not required to drive every element to complete dissolution; instead, the window should prioritize high Mn release, stable slurry handling, and a leachate composition that can be managed downstream.

In this dataset, pushing leaching harder to chase complete Ni dissolution would likely increase time/temperature demands without clear benefit to the Mn product stream. A more practical interpretation is that Ni-bearing phases dissolve more slowly under the tested conditions, and that Ni recovery could be addressed later (for example, by a different leach chemistry or a secondary treatment of residual solids) if it becomes a priority. That separation of objectives keeps the Mn route simpler and reduces the risk of creating a liquor that is harder to clarify or to treat by SX.

Most importantly for integration, chapter 5 shows that the DES-derived leachate produced under this hydration regime could be processed using an established D2EHPA system after straightforward feed preparation (clarification/filtration and pre-contact pH adjustment). In other words, the leaching conditions did not only deliver dissolution; they also delivered liquor that could be conditioned into an SX-compatible feed with stable phase separation and manageable solids carryover. This is why the leaching envelope in chapter 4 should be interpreted as a combined dissolution-and-compatibility result rather than a leaching-only outcome.

6.3 Mn Selectivity in D2EHPA Extraction

Mn extraction with D2EHPA proceeds predominantly via cation exchange (Eq. 5.1), so extraction performance is inherently linked to aqueous acidity. As the pre-contact pH

increases, proton competition decreases and Mn loading improves. However, in a multicomponent feed, higher pH can also increase Co and Ni co-extraction as the organic phase becomes more deprotonated. In this work, the strongest Mn/Co and Mn/Ni separation was obtained at an intermediate pH (≈2.7), where Mn extraction remained high while Co/Ni uptake was still limited.

One practical point in these batch tests is that pH is not static during contacting: as Mn loads by cation exchange, protons are released and the aqueous pH drops. This is why reporting and controlling the pre-contact pH is important, and it also explains why the same nominal starting pH can behave differently when extractant condition or metal loading changes. In a staged circuit, this pH drift would appear as stage-to-stage variation, so future work should track pH profiles across stages rather than only a single bulk value.

Partial saponification provides an additional control handle. Moderate saponification improves Mn loading and reduces the pH drop during extraction, while higher saponification increased the tendency for Co and Ni to load and reduced the separation factors. O/A ratio also has a dual effect: it affects Mn recovery per contact (capacity) and sets the Mn concentration in the loaded organic phase, which then influences stripping efficiency and the strength of the Mn strip liquor. Taken together, the present results support a “window” approach: selectivity comes from jointly tuning pH, saponification, and O/A, rather than maximizing any one variable on its own.

A useful way to interpret the integrated route is through stepwise recovery. Under the optimized batch condition, Mn extraction was 89.7%, followed by 94.8% stripping and 95.3% apparent precipitation recovery, giving an overall Mn recovery of 81.0% to the solid

product. Because the largest single loss occurs in the extraction step (Mn remaining in the raffinate), improving overall recovery while keeping the same selectivity behavior will likely require staged or counter-current extraction operated within the same pH–saponification window, rather than moving to higher pH or higher saponification where Co/Ni co-extraction increases.

Finally, it is notable that this selectivity window was achieved starting from a DES-derived leachate rather than a conventional mineral-acid leach. The practical message is that DES leaching can be paired with established SX chemistry when the liquor is properly clarified and conditioned and when performance is judged using measured stream compositions and a defined product endpoint.

6.4 Process Integration and Scale-up Considerations

The integrated sequence demonstrated here—DES leaching → filtration → pH adjustment → Mn-selective SX → organic washing → two-stage stripping → carbonate precipitation— provides a complete, end-to-end basis for an Mn-forward leach-to-precursor route. Importantly, the steps were demonstrated on the same process logic: the leachate was clarified and conditioned for SX, Mn was transferred and concentrated through stripping, and Mn was finally converted to a handleable $MnCO_3$ solid.

In chapter 5, the separation factors obtained under the optimized conditions were competitive in magnitude with values reported for D2EHPA systems under comparable acidity ranges. In practice, the more meaningful benchmark for this thesis is the integrated outcome: processing a realistic multicomponent liquor, maintaining stable phase behavior

in batch contacting, and producing a verified $MnCO_3$ product stream with quantified stepwise recoveries.

Before the route can be presented as scale-up ready, several validation items should be addressed. These points follow directly from what was measured (and what was not measured) in the present work:

- Stream closure and auditing. Precipitation filtrate and wash waters were not analyzed; therefore, precipitation recovery is reported as an apparent recovery to the recovered $MnCO_3$ solid. Full stream closure is needed to quantify true yields and impurity partitioning.
- Counter-current validation and stage design. Batch experiments establish equilibrium trends but do not define stage requirements, entrainment, phase disengagement kinetics, or third-phase risk. Extraction/stripping isotherms and staged tests are required for McCabe–Thiele design and continuous operation.
- Solvent management and reuse. Sustainability claims depend on demonstrating multi-cycle DES and organic phase reuse, quantifying solvent losses, and controlling water uptake. Hydration improves kinetics but can shift speciation and phase behavior (Aravena et al. 2023; Gabriele et al. 2019; Hammond et al. 2023; Peng et al. 2024).
- Product specification and impurity control. $MnCO_3$ purity should be reported relative to intended end-use requirements, including trace elements and residual anions; additional scrubbing or precipitation-washing optimization may be required.

Overall, the thesis demonstrates an experimentally credible Mn-forward pathway from a sugar-based DES leachate to a confirmed $MnCO_3$ precursor. The next step is to strengthen the process case through mass-balance closure, staged SX validation, and solvent-reuse testing so that the proof-of-concept can be translated into a process-relevant flowsheet.

CHAPTER 7 CONCLUSION, CONTRIBUTION, AND FUTURE STUDIES

7.1 Thesis Conclusions

This thesis developed and demonstrated an Mn "leach-to-precursor" route for spent LIB cathodes by integrating a water-modified sugar-based deep eutectic solvent (DES) (ChCl:D-glucose with 10 wt.% H_2O) with Mn-selective solvent extraction (SX) using D2EHPA and direct carbonate precipitation to $MnCO_3$. The overall outcome is a complete unit-operation sequence—DES leaching, clarification and pH conditioning, Mn-selective SX, organic washing/stripping, and carbonate precipitation—that was tested as a connected process rather than as isolated steps.

In chapter 4, controlled hydration of the ChCl:D-glucose system was shown to be a practical operability lever that improves handling and leaching kinetics relative to the binary DES. Within the investigated operating domain (60–110 °C, 2–24 h, ~10 g L^{-1}), Li and Mn dissolution approached completion (>98%) under optimized conditions, whereas Ni dissolution remained lower (≈71%). These results define a practical leaching envelope for the tested feed and chemistry and show that the water-modified DES can deliver a consistent liquor suitable for downstream processing.

In chapter 5, a fully quantified multicomponent DES-derived leachate (Mn–Co–Ni–Li) was successfully processed using 0.6 M D2EHPA under a defined selectivity window governed primarily by pre-contact pH and partial saponification. Under optimized batch conditions (pre-contact pH 2.7, 25% saponification, O/A ≈ 1), Mn extraction reached 89.7% with limited Co and Ni co-extraction (≈4–6% and 3–5%), corresponding to high separation factors ($\beta Mn/Co = 143$ and $\beta Mn/Ni = 208$). Two-stage acid stripping recovered

94.8% of Mn to an Mn-rich strip liquor, and controlled carbonate precipitation produced $MnCO_3$ with an apparent precipitation recovery of 95.3%, yielding an overall Mn recovery of 81.0% to the solid product. Product identity as rhodochrosite $MnCO_3$ was confirmed by XRD and FTIR. In addition, ICP-based digestion analysis provides the pathway to quantify product composition and residual impurities (including Co, Ni, Fe, Na, and S) in a way that can be linked to precursor-grade requirements once full stream auditing is completed.

Across the integrated route, the stepwise recoveries (89.7% extraction, 94.8% stripping, and 95.3% apparent precipitation recovery) correspond to an overall Mn recovery of 81.0% to the recovered $MnCO_3$ solid under the tested batch conditions. Because precipitation filtrate and wash waters were not analyzed, precipitation recovery is currently reported on an apparent basis; completing stream closure will be important to confirm true yields and to quantify where Mn and impurities partition during washing and filtration.

7.2 Key Contributions

This thesis delivers an Mn-forward "leach-to-precursor" demonstration that links a sugar-based DES leachate to Mn-selective solvent extraction and a verified $MnCO_3$ product. A key achievement is establishing a practical operating envelope for a water-modified ChCl:D-glucose DES (10 wt.% H_2O) that improves operability and supports high Li/Mn dissolution under the investigated time–temperature range. Within this envelope, Li and Mn dissolution approached completion (>98%) under optimized conditions, while Ni dissolution remained lower (≈71%), defining a results-based leaching window suited to an Mn-targeted route rather than an "all-metals" dissolution objective.

A second contribution is the use of an auditable, multicomponent DES-derived liquor for downstream separation, allowing selectivity to be evaluated under real metal–metal competition. The leachate used for SX was fully quantified (Mn 945.6 mg L^{-1}; Co 681.4 mg L^{-1}; Ni 818.3 mg L^{-1}; Li 305.4 mg L^{-1}), and Mn was then selectively recovered with 0.6 M D2EHPA within a clear operating window governed by pre-contact pH and partial saponification. Under the optimized batch condition (pre-contact pH 2.7, 25% saponification, O/A ≈ 1), Mn extraction reached 89.7% with limited Co and Ni co-extraction, giving high separation factors (βMn/Co = 143; βMn/Ni = 208). Two-stage stripping recovered 94.8% of Mn to an Mn-rich strip liquor, and carbonate precipitation produced $MnCO_3$ with an apparent precipitation recovery of 95.3%, corresponding to an overall Mn recovery of 81.0% to the recovered solid.

Finally, the work strengthens "product credibility" by closing the route at a defined precursor endpoint: $MnCO_3$ identity was confirmed by XRD and FTIR, and the overall performance was framed using stepwise metrics (extraction, stripping, precipitation) and a stage-wise Mn mass balance. Together, these results demonstrate that a water-modified glucose DES can be integrated with established D2EHPA chemistry to deliver a quantified, Mn-selective pathway ending in a verified $MnCO_3$ product stream.

7.3 Recommendations for Future Studies

To strengthen process credibility and translate the present batch proof-of-concept into a scalable flowsheet, future work should first establish an auditable stream table with full closure by analyzing all relevant aqueous streams, including precipitation filtrations

and wash waters, as well as organic washing and raffinate streams. This would clarify apparent versus true precipitation recovery, quantify impurity partitioning, and enable rigorous assessment of product-quality drivers. In parallel, scale-up-relevant studies should move from batch separatory-funnel tests to staged operation by determining extraction and stripping isotherms, performing McCabe–Thiele analysis or equivalent stage modeling, and validating counter-current SX performance while monitoring phase disengagement, entrainment, and third-phase risk under higher loadings. A further priority is evaluating solvent and extractant reuse and losses through multi-cycle testing, tracking water uptake and viscosity drift in the DES, monitoring impurity build-up, and quantifying solvent losses to support sustainability and economic claims. Product polishing should also be optimized by refining scrubbing strategies and precipitation parameters (pH trajectory, carbonate addition rate, residence time/aging, and washing protocol) to minimize impurity carryover and tailor $MnCO_3$ properties relevant to precursor-grade specifications. Finally, robustness should be tested on heterogeneous feeds such as true black mass and mixed-chemistry sources, with explicit quantification of how Al/Cu fines and fluorine-containing species influence leaching behavior, SX selectivity, operability, and product quality. Collectively, these studies provide a direct roadmap for translating the integrated DES–SX–precipitation route demonstrated here into a process-relevant Mn recycling flowsheet that reliably delivers $MnCO_3$ as a defined precursor product.

REFERENCES

Abbott, Andrew P., David Boothby, Glen Capper, David L. Davies, and Raymond K. Rasheed. 2004. "Deep Eutectic Solvents Formed between Choline Chloride and Carboxylic Acids: Versatile Alternatives to Ionic Liquids." *Journal of the American Chemical Society* 126(29):9142–47. doi:10.1021/ja048266j.

Abbott, Andrew P., Glen Capper, David L. Davies, Katy J. McKenzie, and Stephen U. Obi. 2006. "Solubility of Metal Oxides in Deep Eutectic Solvents Based on Choline Chloride." *Journal of Chemical and Engineering Data* 51(4):1280–82. doi:10.1021/je060038c.

Aravena, Paulo, Esteban Cea-Klapp, Nicolás F. Gajardo-Parra, Christoph Held, José Matías Garrido, and Roberto I. Canales. 2023. "Effect of Water and Hydrogen Bond Acceptor on the Density and Viscosity of Glycol-Based Eutectic Solvents." *Journal of Molecular Liquids* 389. doi:10.1016/j.molliq.2023.122856.

Asadi Dalini, E., Gh Karimi, S. Zandevakili, and M. Goodarzi. 2020. "A Review on Environmental, Economic and Hydrometallurgical Processes of Recycling Spent Lithium-Ion Batteries." *Mineral Processing and Extractive Metallurgy Review* 42(7):1–22. doi:10.1080/08827508.2020.1781628.

Baum, Zachary J., Robert E. Bird, Xiang Yu, and Jia Ma. 2022. "Lithium-Ion Battery Recycling─Overview of Techniques and Trends." *ACS Energy Letters* 7(2):712–19. doi:10.1021/acsenergylett.1c02602.

Behnajady, B., J. Yousefi Seyf, S. Karimi, M. Moradi, and M. Sohrabi. 2024. "Molecular Dynamic (MD) Simulation and Density Function Theory (DFT) Calculation Relevant to Green Leaching of Metals from Spent Lithium-Ion Battery Cathode Materials Using Glucose-Based Deep Eutectic Solvent (DES)." *Hydrometallurgy* 223. doi:10.1016/j.hydromet.2023.106223.

Buken, Onurcan, Kayla Mancini, and Amrita Sarkar. 2021. "A Sustainable Approach to Cathode Delamination Using a Green Solvent." *RSC Advances* 11(44):27356–68. doi:10.1039/D1RA04922D.

Chan, Ka Ho, John Anawati, Monu Malik, and Gisele Azimi. 2021. "Closed-Loop Recycling of Lithium, Cobalt, Nickel, and Manganese from Waste Lithium-Ion Batteries of Electric Vehicles." *ACS Sustainable Chemistry and Engineering* 9(12):4398–4410. doi:10.1021/acssuschemeng.0c06869.

Chang, Xin, Min Fan, Chao Fan Gu, Wei Huan He, Qinghai Meng, Li Jun Wan, and Yu Guo Guo. 2022. “Selective Extraction of Transition Metals from Spent LiNixCoyMnx1−−yO2 Cathode via Regulation of Coordination Environment.” *Angewandte Chemie - International Edition* 61(24). doi:10.1002/anie.202202558.

Chen, Yu, Fuguang Zhang, Cheng Yang, Xiaoge Ju, Ziyang Zhang, Zhenghui Liu, and Mingshuai Yang. 2024. “Efficient and Selective Dissolution of Li from Lithium-Ion Battery LiFePO4 Cathode by Natural Deep Eutectic Solvents.” *Energy and Fuels* 38(6):5391–96. doi:10.1021/acs.energyfuels.4c00080.

Cornelio, Antonella, Alessandra Zanoletti, and Elza Bontempi. 2024. “Recent Progress in Pyrometallurgy for the Recovery of Spent Lithium-Ion Batteries: A Review of State-of-the-Art Developments.” *Current Opinion in Green and Sustainable Chemistry* 46.

Dai, Yuntao, Jaap van Spronsen, Geert Jan Witkamp, Robert Verpoorte, and Young Hae Choi. 2013. “Natural Deep Eutectic Solvents as New Potential Media for Green Technology.” *Analytica Chimica Acta* 766:61–68. doi:10.1016/j.aca.2012.12.019.

Dong, Liping, Yongjian Li, Pei Shi, Zhongqi Ren, and Zhiyong Zhou. 2023. “Low-Viscosity Acidic Deep Eutectic Solvent for Extraction of Valuable Metals from Spent NCM.” *Journal of Power Sources* 582:233564. doi:10.1016/j.jpowsour.2023.233564.

Dorella, Germano, and Marcelo Borges Mansur. 2007. “A Study of the Separation of Cobalt from Spent Li-Ion Battery Residues.” *Journal of Power Sources* 170(1):210–15. doi:10.1016/j.jpowsour.2007.04.025.

Fan, Yuxin, Yuelin Kong, Pinxian Jiang, Guohua Zhang, Jianlong Cong, Xinyue Shi, Yukun Liu, Ping Zhang, Renyuan Zhang, and Yunhui Huang. 2023. “Development and Challenges of Deep Eutectic Solvents for Cathode Recycling of End-of-Life Lithium-Ion Batteries.” *Chemical Engineering Journal* 463. doi:10.1016/j.cej.2023.142278.

Gabriele, Francesco, M. Chiarini, Raimondo Germani, Matteo Tiecco, and Nicoletta Spreti. 2019. “Effect of Water Addition on Choline Chloride/Glycol Deep Eutectic Solvents: Characterization of Their Structural and Physicochemical Properties.” *Journal of Molecular Liquids* 291. doi:10.1016/j.molliq.2019.111301.

Gaines, Linda. 2018. “Lithium-Ion Battery Recycling Processes: Research towards a Sustainable Course.” *Sustainable Materials and Technologies* 17:e00068. doi:10.1016/j.susmat.2018.e00068.

Gilligan, Rorie, Glen P. O’Malley, and Aleksandar N. Nikoloski. 2025. “The Leaching of Valuable Metals (Li, Co, Ni, Mn, Cu) from Black Mass from Spent Lithium-Ion Batteries.” *Metals* 15(10):1155. doi:10.3390/met15101155.

Golmohammadzadeh, Rabeeh, Fereshteh Rashchi, and Ehsan Vahidi. 2017. “Recovery of Lithium and Cobalt from Spent Lithium-Ion Batteries Using Organic Acids: Process Optimization and Kinetic Aspects.” *Waste Management* 64:244–54. doi:10.1016/j.wasman.2017.03.037.

Goudarzi, Jafar, Zhi Chen, Gaixia Zhang, Jinguang Hu, Karim Zaghib, Sixu Deng, Afzal Ahmed Dar, Xiaolei Wang, Fariborz Haghighat, Catherine N. Mulligan, Chunjiang An, and Antonio Avalos Ramirez. 2025. “Sustainable Recovery of Critical Metals from Spent Lithium-Ion Batteries Using Deep Eutectic Solvents.” *Batteries* 11(9):340. doi:10.3390/batteries11090340.

Gygli, Gudrun, Xinmeng Xu, and Jürgen Pleiss. 2020. “Meta-Analysis of Viscosity of Aqueous Deep Eutectic Solvents and Their Components.” *Scientific Reports* 10(1):21395. doi:10.1038/s41598-020-78101-y.

Hammond, Oliver S., Elly K. Bathke, Daniel T. Bowron, and Karen J. Edler. 2023. “Trace Water Changes Metal Ion Speciation in Deep Eutectic Solvents: Ce 3+ Solvation and Nanoscale Water Clustering in Choline Chloride–Urea–Water Mixtures.” *Inorganic Chemistry* 62(44):18069–78. doi:10.1021/acs.inorgchem.3c02205.

Harper, Gavin, Roberto Sommerville, Emma Kendrick, Laura Driscoll, Peter Slater, Rustam Stolkin, Allan Walton, Paul Christensen, Oliver Heidrich, Simon Lambert, Andrew Abbott, Karl Ryder, Linda Gaines, and Paul Anderson. 2019. “Recycling Lithium-Ion Batteries from Electric Vehicles.” *Nature* 575(7781):75–86. doi:10.1038/s41586-019-1682-5.

Jantunen, Niklas, Sami Virolainen, and Tuomo Sainio. 2022. “Direct Production of Ni–Co–Mn Mixtures for Cathode Precursors from Cobalt-Rich Lithium-Ion Battery Leachates by Solvent Extraction.” *Metals* 12(9):1445. doi:10.3390/met12091445.

Ji, Yi, Chad T. Jafvert, Nadezhda N. Zyaykina, and Fu Zhao. 2022. “Decomposition of PVDF to Delaminate Cathode Materials from End-of-Life Lithium-Ion Battery Cathodes.” *Journal of Cleaner Production* 367:133112. doi:10.1016/j.jclepro.2022.133112.

Kang, Jingu, Gamini Senanayake, Jeongsoo Sohn, and Shun Myung Shin. 2010. “Recovery of Cobalt Sulfate from Spent Lithium Ion Batteries by Reductive Leaching and Solvent Extraction with Cyanex 272.” *Hydrometallurgy* 100(3–4):168–71. doi:10.1016/j.hydromet.2009.10.010.

Keller, A., M. W. Hlawitschka, and H. J. Bart. 2021. “Manganese Recycling of Spent Lithium Ion Batteries via Solvent Extraction.” *Separation and Purification Technology* 275. doi:10.1016/j.seppur.2021.119166.

Keller, A., M. W. Hlawitschka, and H. J. Bart. 2022. “Application of Saponified D2EHPA for the Selective Extraction of Manganese from Spent Lithium-Ion Batteries.” *Chemical Engineering and Processing - Process Intensification* 171:108552. doi:10.1016/j.cep.2021.108552.

Kim, Seoa, Jaeyeon Bang, Junsang Yoo, Youngjun Shin, Jihyeon Bae, Juyeon Jeong, Kyumin Kim, Peng Dong, and Kyungjung Kwon. 2021. “A Comprehensive Review on the Pretreatment Process in Lithium-Ion Battery Recycling.” *Journal of Cleaner Production* 294.

Kivelä, Henri, Mikko Salomäki, Petteri Vainikka, Ermei Mäkilä, Fabrizio Poletti, Stefano Ruggeri, Fabio Terzi, and Jukka Lukkari. 2022. “Effect of Water on a Hydrophobic Deep Eutectic Solvent.” *The Journal of Physical Chemistry B* 126(2):513–27. doi:10.1021/acs.jpcb.1c08170.

Latini, Dario, Marco Vaccari, Marco Lagnoni, Martina Orefice, Fabrice Mathieux, Jaco Huisman, Leonardo Tognotti, and Antonio Bertei. 2022. “A Comprehensive Review and Classification of Unit Operations with Assessment of Outputs Quality in Lithium-Ion Battery Recycling.” *Journal of Power Sources* 546:231979. doi:10.1016/j.jpowsour.2022.231979.

Lei, Chunhong, Iain Aldous, Jennifer M. Hartley, Dana L. Thompson, Sean Scott, Rowan Hanson, Paul A. Anderson, Emma Kendrick, Rob Sommerville, Karl S. Ryder, and Andrew P. Abbott. 2021. “Lithium Ion Battery Recycling Using High-Intensity Ultrasonication.” *Green Chemistry* 23(13):4710–15. doi:10.1039/D1GC01623G.

Lei, Shuya, Wei Sun, and Yue Yang. 2022. “Solvent Extraction for Recycling of Spent Lithium-Ion Batteries.” *Journal of Hazardous Materials* 424.

Locati, Andrea, Maja Mikulić, Léa M. J. Rouquette, Burçak Ebin, and Martina Petranikova. 2024. “Production of High Purity MnSO4·H2O from Real NMC111 Lithium-Ion Batteries Leachate Using Solvent Extraction and Evaporative Crystallization.” *Solvent Extraction and Ion Exchange* 42(6–7):636–57. doi:10.1080/07366299.2024.2435272.

Luo, Yi, Chengzhe Yin, Leming Ou, and Chenyang Zhang. 2022. “Highly Efficient Dissolution of the Cathode Materials of Spent Ni–Co–Mn Lithium Batteries Using Deep Eutectic Solvents.” *Green Chemistry* 24(17):6562–70. doi:10.1039/D2GC01431A.

Ma, Yunping, Yu Yang, Tie Li, Shahid Hussain, and Maiyong Zhu. 2024. “Deep Eutectic Solvents as an Emerging Green Platform for the Synthesis of Functional Materials.” *Green Chemistry* 26(7):3627–69. doi:10.1039/d3gc04289h.

Makuza, Brian, Qinghua Tian, Xueyi Guo, Kinnor Chattopadhyay, and Dawei Yu. 2021. "Pyrometallurgical Options for Recycling Spent Lithium-Ion Batteries: A Comprehensive Review." *Journal of Power Sources* 491.

Martín, M. I., I. García-Díaz, and F. A. López. 2023. "Properties and Perspective of Using Deep Eutectic Solvents for Hydrometallurgy Metal Recovery." *Minerals Engineering* 203.

Meredith, Leon, Aaron Elbourne, Tamar L. Greaves, Gary Bryant, and Saffron J. Bryant. 2024. "Physico-Chemical Characterisation of Glycerol- and Ethylene Glycol-Based Deep Eutectic Solvents." *Journal of Molecular Liquids* 394. doi:10.1016/j.molliq.2023.123777.

Milian, Yanio E., Nathalie Jamett, Constanza Cruz, Sebastián Herrera-León, and Jaime Chacana-Olivares. 2024. "A Comprehensive Review of Emerging Technologies for Recycling Spent Lithium-Ion Batteries." *Science of the Total Environment* 910(August 2023). doi:10.1016/j.scitotenv.2023.168543.

Nadimi, H., and N. Jalalian Karazmoudeh. 2021. "Selective Separation and Purification of Mn from Co and Ni in Waste Mobile Phone Lithium-Ion Batteries Using D2EHPA via Solvent Extraction Method." *Journal of Sustainable Metallurgy* 7(2):653–63. doi:10.1007/s40831-021-00371-1.

Neumann, Jonas, Martina Petranikova, Marcel Meeus, Jorge D. Gamarra, Reza Younesi, Martin Winter, and Sascha Nowak. 2022. "Recycling of Lithium-Ion Batteries—Current State of the Art, Circular Economy, and Next Generation Recycling." *Advanced Energy Materials* 12(17). doi:10.1002/aenm.202102917.

Ojanen, Severi, Mari Lundström, Annukka Santasalo-Aarnio, and Rodrigo Serna-Guerrero. 2018. "Challenging the Concept of Electrochemical Discharge Using Salt Solutions for Lithium-Ion Batteries Recycling." *Waste Management* 76:242–49. doi:10.1016/j.wasman.2018.03.045.

Or, Tyler, Storm W. D. Gourley, Karthikeyan Kaliyappan, Aiping Yu, and Zhongwei Chen. 2020. "Recycling of Mixed Cathode Lithium-Ion Batteries for Electric Vehicles: Current Status and Future Outlook." *Carbon Energy* 2(1):6–43.

Padwal, Chinmayee, Hong Duc Pham, Sagar Jadhav, Thu Trang Do, Jawahar Nerkar, Linh Thi My Hoang, Ashok Kumar Nanjundan, Sagadevan G. Mundree, and Deepak P. Dubal. 2022. "Deep Eutectic Solvents: Green Approach for Cathode Recycling of Li-Ion Batteries." *Advanced Energy and Sustainability Research* 3(1). doi:10.1002/aesr.202100133.

Peeters, Nand, Koen Binnemans, and Sofía Riaño. 2020. “Solvometallurgical Recovery of Cobalt from Lithium-Ion Battery Cathode Materials Using Deep-Eutectic Solvents.” *Green Chemistry* 22(13):4210–21. doi:10.1039/d0gc00940g.

Peng, Daili, Zhen Yu, Ahmad Alhadid, and Mirjana Minceva. 2024. “Modeling the Viscosity of ChCl-Based Deep Eutectic Solvents and Their Mixtures with Water.” *Industrial and Engineering Chemistry Research* 63(3):1623–33. doi:10.1021/acs.iecr.3c03652.

Rautela, Rahul, Bholu Ram Yadav, and Sunil Kumar. 2023. “A Review on Technologies for Recovery of Metals from Waste Lithium-Ion Batteries.” *Journal of Power Sources* 580:233428. doi:10.1016/j.jpowsour.2023.233428.

Rehman, Sheikh, Maher Al-Greer, Adam S. Burn, Michael Short, and Xinjun Cui. 2025. “High-Volume Battery Recycling: Technical Review of Challenges and Future Directions.” *Batteries* 11(3).

Ren, Liuyi, Bo Liu, Shenxu Bao, Wei Ding, Yimin Zhang, Xiaochuan Hou, Chao Lin, and Bo Chen. 2024. “Recovery of Li, Ni, Co and Mn from Spent Lithium-Ion Batteries Assisted by Organic Acids: Process Optimization and Leaching Mechanism.” *International Journal of Minerals, Metallurgy and Materials* 31(3):518–30. doi:10.1007/s12613-023-2735-1.

Rensmo, Amanda, Eleni K. Savvidou, Ian T. Cousins, Xianfeng Hu, Steffen Schellenberger, and Jonathan P. Benskin. 2023. “Lithium-Ion Battery Recycling: A Source of per- and Polyfluoroalkyl Substances (PFAS) to the Environment?” *Environmental Science: Processes & Impacts* 25(6):1015–30. doi:10.1039/D2EM00511E.

Rouquette, Léa M. J., Martina Petranikova, and Nathália Vieceli. 2023. “Complete and Selective Recovery of Lithium from EV Lithium-Ion Batteries: Modeling and Optimization Using Oxalic Acid as a Leaching Agent.” *Separation and Purification Technology* 320. doi:10.1016/j.seppur.2023.124143.

Rozas, Sara, Cristina Benito, Rafael Alcalde, Mert Atilhan, and Santiago Aparicio. 2021. “Insights on the Water Effect on Deep Eutectic Solvents Properties and Structuring : The Archetypical Case of Choline Chloride + Ethylene Glycol.” *Journal of Molecular Liquids* 344:117717. doi:10.1016/j.molliq.2021.117717.

Seyf, Jaber Yousefi, and Fatemeh Zarei. 2022. “Density, Viscosity, and Refractive Index of a Choline Chloride + d -(-)-Fructose Deep Eutectic Solvent + Water Mixture at Different Temperatures: An Experimental Study and Thermodynamic Modeling.”

Journal of Chemical and Engineering Data 67(10):3007–21. doi:10.1021/acs.jced.2c00440.

Shaibuna, M., Letcy V. Theresa, and K. Sreekumar. 2022. "Neoteric Deep Eutectic Solvents: History, Recent Developments, and Catalytic Applications." *Soft Matter* 18(14):2695–2721.

Shaw-Stewart, James, Anna Alvarez-Reguera, Agata Greszta, James Marco, Maryam Masood, Rob Sommerville, and Emma Kendrick. 2019. "Aqueous Solution Discharge of Cylindrical Lithium-Ion Cells." *Sustainable Materials and Technologies* 22:e00110. doi:10.1016/j.susmat.2019.e00110.

Shin, Shun Myung, Nak Hyoung Kim, Jeong Soo Sohn, Dong Hyo Yang, and Young Han Kim. 2005. "Development of a Metal Recovery Process from Li-Ion Battery Wastes." *Hydrometallurgy* 79(3–4):172–81. doi:10.1016/j.hydromet.2005.06.004.

Smith, Emma L., Andrew P. Abbott, and Karl S. Ryder. 2014. "Deep Eutectic Solvents (DESs) and Their Applications." *Chemical Reviews* 114(21):11060–82.

Srivastava, Varsha, Venla Rantala, Parisa Mehdipour, Toni Kauppinen, Sari Tuomikoski, Anne Heponiemi, Hanna Runtti, Pekka Tynjälä, Glaydson Simões Dos Reis, and Ulla Lassi. 2023. "A Comprehensive Review of the Reclamation of Resources from Spent Lithium-Ion Batteries." *Chemical Engineering Journal* 474(September). doi:10.1016/j.cej.2023.145822.

Su, Runchang, Shujie Tang, Mei Zhang, and Min Guo. 2024. "Strategies for Overcoming Challenges in Using Deep Eutectic Solvents for the Selective Extraction of Valuable Metals from Spent Lithium-Ion Batteries: A Review." *Journal of Environmental Chemical Engineering* 12(4):113200. doi:10.1016/j.jece.2024.113200.

Takahashi, V. C. I., A. B. Botelho Junior, D. C. R. Espinosa, and J. A. S. Tenório. 2020. "Enhancing Cobalt Recovery from Li-Ion Batteries Using Grinding Treatment Prior to the Leaching and Solvent Extraction Process." *Journal of Environmental Chemical Engineering* 8(3). doi:10.1016/j.jece.2020.103801.

Tang, Shujie, Jiali Feng, Runchang Su, Mei Zhang, and Min Guo. 2022. "New Bifunctional Deep-Eutectic Solvent for In Situ Selective Extraction of Valuable Metals from Spent Lithium Batteries." *ACS Sustainable Chemistry & Engineering* 10(26):8423–32. doi:10.1021/acssuschemeng.2c01408.

Tran, Mai K., Marco Tulio F. Rodrigues, Keiko Kato, Ganguli Babu, and Pulickel M. Ajayan. 2019. "Deep Eutectic Solvents for Cathode Recycling of Li-Ion Batteries." *Nature Energy* 4(4):339–45. doi:10.1038/s41560-019-0368-4.

Velázquez-Martínez, Omar, Johanna Valio, Annukka Santasalo-Aarnio, Markus Reuter, and Rodrigo Serna-Guerrero. 2019. "A Critical Review of Lithium-Ion Battery Recycling Processes from a Circular Economy Perspective." *Batteries* 5(4):68. doi:10.3390/batteries5040068.

Vieceli, Nathália, Niclas Reinhardt, Christian Ekberg, and Martina Petranikova. 2020. "Optimization of Manganese Recovery from a Solution Based on Lithium-Ion Batteries by Solvent Extraction with D2EHPA." doi:.

Wang, Chao, Shubin Wang, Feng Yan, Zhen Zhang, Xuehua Shen, and Zuotai Zhang. 2020. "Recycling of Spent Lithium-Ion Batteries: Selective Ammonia Leaching of Valuable Metals and Simultaneous Synthesis of High-Purity Manganese Carbonate." *Waste Management* 114:253–62. doi:10.1016/j.wasman.2020.07.008.

Wang, Jingxiu, Yanqiu Lyu, Rong Zeng, Shilin Zhang, Kenneth Davey, Jianfeng Mao, and Zaiping Guo. 2023. "Green Recycling of Spent Li-Ion Battery Cathodes via Deep-Eutectic Solvents." *Energy and Environmental Science* 17(3):867–84.

Wang, Shubin, Zuotai Zhang, Zhouguang Lu, and Zhenghe Xu. 2020. "A Novel Method for Screening Deep Eutectic Solvent to Recycle the Cathode of Li-Ion Batteries." *Green Chemistry* 22(14):4473–82. doi:10.1039/d0gc00701c.

Wang, Yuqing, Ning An, Lei Wen, Lei Wang, Xiaotong Jiang, Feng Hou, Yuxin Yin, and Ji Liang. 2020. "Recent Progress on the Recycling Technology of Li-Ion Batteries." *Journal of Energy Chemistry* 55:391–419.

Xu, Kang. 2004. "Nonaqueous Liquid Electrolytes for Lithium-Based Rechargeable Batteries." *Chemical Reviews* 104(10):4303–4418. doi:10.1021/cr030203g.

Yun, Seol Ho, Jiang Xian Wen, and Man Seung Lee. 2024. "Separation of Co(II), Mn(II), and Ni(II) by Solvent Extraction with Cyanex 272 and D2EHPA from the Sulfuric Acid Leaching Solution of Spent Lithium-Ion Batteries." *Physicochemical Problems of Mineral Processing* 60(5). doi:10.37190/PPMP/193742.

Zhang, Guangwen, Xue Yuan, Yaqun He, Haifeng Wang, Tao Zhang, and Weining Xie. 2021. "Recent Advances in Pretreating Technology for Recycling Valuable Metals from Spent Lithium-Ion Batteries." *Journal of Hazardous Materials* 406.

Zhang, Kuifang, Helei Liang, Xiaocong Zhong, Hongyang Cao, Ruixiang Wang, and Zhiqiang Liu. 2022. "Recovery of Metals from Sulfate Leach Solutions of Spent Ternary Lithium-Ion Batteries by Precipitation with Phosphate and Solvent Extraction with P507." *Hydrometallurgy* 210(March):105861. doi:10.1016/j.hydromet.2022.105861.

Zhang, Qinghua, Karine De Oliveira Vigier, Sébastien Royer, and François Jérôme. 2012. "Deep Eutectic Solvents: Syntheses, Properties and Applications." *Chemical Society Reviews* 41(21):7108–46. doi:10.1039/c2cs35178a.

Zhu, Ahui, Xinyu Bian, Weijiang Han, Dianxue Cao, Yong Wen, Kai Zhu, and Shubin Wang. 2023. "The Application of Deep Eutectic Solvents in Lithium-Ion Battery Recycling: A Comprehensive Review." *Resources, Conservation and Recycling* 188:106690. doi:10.1016/j.resconrec.2022.106690.